Facies and architectural asymmetry of a submarine channel fill, Cerro Toro Formation, Chile

# FACIES AND ARCHITECTURAL ASYMMETRY IN A CONGLOMERATE-RICH SUBMARINE CHANNEL FILL, CERRO TORO FORMATION, SIERRA DEL TORO, MAGALLANES BASIN, CHILE

**ZANE R. JOBE, ANNE BERNHARDT, AND DONALD R. LOWE**

zanejobe@gmail.com

Phone: 650 723 0848

Fax: 650 725 0979

Affiliation, all authors: Department of Geological and Environmental Sciences, Stanford University; 450 Serra Mall, Building 320, Stanford, California, 94305, U.S.A.

Keywords: sinuous submarine channel-levee complex; submarine canyon; transitional sediment gravity flow; lateral accretion; knickpoint

## ABSTRACT

Cross-sectional asymmetry is characteristic of sinuous channels, in both fluvial and submarine settings. Less well documented are the facies distributions of

asymmetric channels, particularly in submarine settings. Exposures of the axial channel-belt in the Magallanes retro-arc foreland basin on Sierra del Toro represent the fill of a 3.5 km wide, 300 m thick channel complex, here termed the "Wildcat," that displays an asymmetric cross section and facies distribution. Measured sections and mapping demonstrate that facies proportion, degree of amalgamation, and margin architecture vary laterally from east to west across the Wildcat channel complex. The eastern side is characterized by thick-bedded, amalgamated sandstone and clast- and matrix-supported conglomerate that onlap a steep, simple margin adjacent to sandy overbank deposits. The western side contains thin-bedded, sandy and muddy strata that onlap a shallow composite margin adjacent to mud-rich out-of-channel strata.

The observed asymmetry is likely due to centrifugal flow forces and was caused by a low-sinuosity right-hand meander bend of the Cerro Toro axial channel-belt. The facies and architecture of the opposing margins indicate that the eastern and western sides constitute the outer and inner bends of the Wildcat channel complex, respectively. The modest cross-sectional asymmetry of the Wildcat complex is likely a product of the low channel-belt sinuosity. The absence of lateral accretion surfaces and deposits suggests that the channel did not migrate during filling. Flows depositing the uppermost channel fill were only weakly confined, resulting in flow divergence and overbank deposition.

A depositional model that incorporates the asymmetric facies distributions and the contrasting outer-bend and inner-bend architecture of the Wildcat channel complex is also presented. Similar facies distributions exist in other low-sinuosity submarine channels, and even more extreme facies and cross-sectional asymmetry probably characterize more highly sinuous channels. Data on facies distributions presented here represents a useful resource for constraining numerical and experimental models of the evolution of sinuous submarine channels as well as reservoir models of sinuous submarine channels.

## INTRODUCTION

Channel asymmetry can be defined both by the cross-sectional shape of the channel, or *architectural asymmetry*, and by the across-channel variation in infilling grain size and facies, or *facies asymmetry* (Pyles et al. 2010). Generally, sinuosity and asymmetry are highly correlated (Melton 1936). Leopold and Wolman (1960) provide a thorough review of this bifold asymmetry for meandering fluvial systems, and more recent studies include Nanson (1980), LaPointe and Carson (1986), Johanneson and Parker (1989), Miall (1996), and Dodov and Foufoula-Georgiou (2004). Architectural asymmetry is caused by enhanced erosion of the outer bank of a channel due to differential boundary shear stress generated as a flow negotiates a meander bend. Higher sinuosities, therefore, generate a steep outer bank and a shallow inner bank at

bend apices, whereas channels with lower sinuosities tend to be only slightly asymmetric at bend apices. At inflection points between bends or at straight reaches of channels, symmetric cross-sections are expected (Pyles et al. 2010). Facies asymmetry is caused by flow-velocity gradients as well as helical flow patterns redistributing sediment across the channel (see Leopold and Wolman 1960 and references therein).

Architecturally asymmetric submarine channels were not identified until high-resolution bathymetric data became available. First recognized were the higher outer-bank levees (Buffington 1952; Flood and Damuth 1987) caused by flow superelevation (Imran et al. 1999), Coriolis forces (Menard 1955; Klaucke et al. 1998) or fold-belt development (Clark and Cartwright 2009). Seismic-reflection (Kolla et al. 2001), outcrop (Satur et al. 2005; Pyles et al. 2010), and modern-seafloor studies (Hay 1987a, 1987b; Babonneau et al. 2002; Antobreh and Krastel 2006; Lamb et al. 2008) confirm the widespread architectural asymmetry of sinuous submarine channels.

Facies asymmetry has been more widely recognized in submarine channels due to outcrop access and the focus of the petroleum industry on intrachannel reservoir communication. Seismic-reflection studies commonly describe facies asymmetry in submarine channels, both with (Stelting et al. 1985a; Stelting et al. 1985b; De Ruig and Hubbard 2006) and without (Abreu et al. 2003; Deptuck et al. 2003; Kolla et al. 2007) lithologic calibration. Outcrop studies also describe submarine channel-fill exhibiting facies asymmetry (Campion et al. 2000; Hickson and Lowe 2002; Abreu et al. 2003; Satur

et al. 2005; Crane and Lowe 2008; Pyles et al. 2010). At least two sinuous modern submarine channels have been cored that demonstrate facies asymmetry (Hay et al. 1983a,1983 b; Johnson et al. 2009). These numerous examples of architectural and facies asymmetry, however, are rarely considered when making reservoir models (Labourdette 2007; Sweet and Sumpter 2007). Many flume studies also reproduce facies asymmetry in sinuous channels (Keevil et al. 2006; Keevil et al. 2007; Straub et al. 2008), but these channels are built with symmetric U-shaped cross-sections, questioning their validity.

Outcrops of the Cerro Toro Formation in southern Chile provide both continuous, three-dimensional bed-scale exposure and the larger context of the overall depositional system necessary to construct accurate models of the architecture and evolution of asymmetric submarine channels. This study reports the large (3.5 km wide x 6 km long x 300 m thick), well exposed, very coarse-grained "Wildcat" channel complex on Sierra del Toro, emphasizing the asymmetric facies distribution. The architectural asymmetry is minimal, likely due to the very low sinuosity. A depositional model for sinuous submarine channels is presented, based on observed lateral and downdip variations in facies proportion, degree of amalgamation, paleoflow, and margin architecture. This model can be widely applicable and, combined with data from other similar systems, may be used to predict the sinuosity and planform characteristics of asymmetric submarine channels. The quantitative

lithologic data, such as amalgamation ratio and facies proportions, can also be used to populate more realistic models of reservoir heterogeneity and constrain numerical and experimental models of submarine channels.

## MAGALLANES FORELAND BASIN, SOUTHERN CHILE

The Magallanes retro-arc foreland basin (Fig. 1) was created as a result of the inversion of the Rocas Verdes back-arc basin, a rift basin associated with Gondwana breakup (Biddle et al. 1986). Basin inversion was caused by the onset of Andean compressional orogenesis and flexural loading at 92 Ma (Wilson 1991; Fildani et al. 2003; Fildani and Hessler 2005), marked in the Ultima Esperanza district of southern Chile (Fig. 1B) by the deposition of the Punta Barrosa Formation (Fig. 1C). Subsidence rates were high due to the extended crustal underpinnings of the basin (Dalziel et al. 1974) and were intensified by orogenic loading (Fig. 1D; Wilson 1991). Thus, the Magallanes basin remained underfilled and at bathyal water depth (Katz 1963; Natland et al. 1974; Wilson 1991; Fildani and Hessler 2005) during deposition of the Coniacian-Campanian Cerro Toro Formation (Fig. 1C; Katz 1963, Scott 1966). The Cerro Toro Formation consists of more than 2000 m of turbiditic mudstone, but lenses of conglomerate and sandstone up to 400 m thick (the "Lago Sofia" member) are encased within this mudstone (Zeil 1958; Scott 1966; Winn and Dott 1979). These coarse-grained deposits are remnants of a southward-flowing conglomeratic channel-belt that occupied

the axis of the elongate foreland basin (Hubbard et al. 2008). Overlying the Cerro Toro Formation is the Tres Pasos Formation, a major slope system (Macellari et al. 1989; Shultz et al. 2005; Hubbard et al. 2010) displaying channelized submarine fans and/or lobes (Romans et al. 2009a), mass-transport deposits (Armitage et al. 2009), and ponded mini-basin fills (Shultz and Hubbard 2005). The Dorotea Formation overlies the Tres Pasos Formation (Macellari et al. 1989) and represents a shelf-edge delta that fed the Tres Pasos slope system (Covault et al. 2009; Hubbard et al. 2010). Extensive reviews of the tectonic and sedimentary evolution of the Magallanes basin are provided by Fildani et al. (2008) and Bernhardt et al. (2008), respectively.

## AXIAL CHANNEL-BELT OF THE CERRO TORO FORMATION

First mapped in the early twentieth century (Hauthal 1907), the conglomeratic lenses of the Cerro Toro Formation represent the deposits of an axial channel-belt that was more than 100 km in length and ~ 8 km wide (Hubbard et al. 2008). Scott (1966) first described the conglomerate units as deep-water units deposited by southward-flowing currents. Winn and Dott (1977, 1979) interpreted the formation as a leveed-channel system deposited by southward-moving turbidity flows on an elongate submarine fan. The most recent interpretation (Hubbard et al. 2008) is that the ~ 400-m-thick Lago Sofia member represents an axial channel-belt partially confined by levees and partially by the foredeep margin. This channel belt displayed very low (1.06)

sinuosity and likely had multiple tributary conduits (Fig. 1; Crane and Lowe 2008; Hubbard et al. 2008). Provenance of the channel-belt fill is interpreted to be the Andean arc and fold-and-thrust belt; sandstone plots in the *transitional arc* QFL domain and conglomerate clasts consist predominantly of rhyolites, granitoids, and metasedimentary rocks (Zeil 1958; Scott 1966; Crane 2004; Valenzuela 2006). Romans et al. (2009b) provides a comprehensive provenance analysis of the axial channel-belt and the rest of the Magallanes basin.

### *Paleogeography of the Axial Channel-Belt*

A paleogeographic reconstruction of the Magallanes basin during deposition of the Cerro Toro axial channel-belt is shown in Figure 1A. The coarse, up to boulder, grain size and amalgamated facies relationships of the channel-belt deposits suggest that the source area had high sediment supply, a steep gradient, and a narrow shelf. Coeval shallow-marine deposits identified about 50 km north of the study area are thought to represent a coeval coastal system that fed sediment into the channel belt (Macellari et al. 1989); however, these deposits have not been studied in detail. A modern analog for the Cerro Toro axial channel-belt is the Gaoping submarine canyon and Manila trench submarine channel system in the foreland basin of SW Taiwan, which is a river-fed, high sediment-supply, high-gradient system (Yu et al. 2009). An excellent subsurface analog is the Puchkirchen axial channel-belt in the Molasse pro-

foreland basin of Austria, which displays dimensions, grain size, and architecture similar to the Cerro Toro axial channel-belt (De Ruig and Hubbard 2006; Hubbard et al. 2008; Hubbard et al. 2009). The Cerro Toro axial channel-belt extended for more than 200 km to the south, into Tierra del Fuego (Dott et al. 1982). Proximal parts of the Cerro Toro axial channel-belt are exposed at Sierra del Toro (Fig. 1B), the focus of this study. Downslope exposures to the south include the Cordillera Manuel Señoret and Cerro Rotunda (Hubbard et al. 2008). The Silla Syncline (Fig. 1B), a western locale of proximal Cerro Toro conglomeratic channel-fill, may represent a tributary channel to the axial channel-belt or the prior location of the belt due to foredeep migration (Crane and Lowe 2008; Bernhardt et al. in press).

### *Cordillera Manuel Señoret*

Outcrops of the Cerro Toro Formation in the Cordillera Manuel Señoret area (Fig. 1B) contain highly amalgamated conglomerate and sandstone incised into turbiditic mudstone (Winn and Dott 1979; Hubbard et al. 2008). Winn and Dott (1977) describe dunes with 4 m of relief from this part of the channel belt. Hubbard et al. (2008) undertook a comprehensive study of the area and suggested that confinement was provided both by inner levees and the foredeep margin. Hubbard et al. (2008) presented clear evidence for inner-levee development at channel margins on both sides of the channel belt, including overbank diverging paleoflow, bed thinning away from

the channel, and slumps associated with levee topography. The narrowing of the outcrop belt and the downdip increase in amalgamation are suggested by Hubbard et al. (2008) to represent a constriction of the foredeep concurrent with deposition caused by differential Andean thrusting.

### *Sierra del Toro*

The study area, Sierra del Toro, is a mountain range near the northern, proximal end of the outcrop exposure of the Cerro Toro axial channel-belt (Figs. 1, 2) and is approximately 100 $km^2$ in areal extent and 1300 m in relief (Fig. 2). Scott (1966) first noted the presence of conglomerate and south-directed paleocurrents on Sierra del Toro. On the basis of facies relationships and foraminiferal assemblages, Winn and Dott (1979) later interpreted conglomerate packages on Sierra del Toro as part of an elongate, leveed submarine fan-channel system. Hubbard et al. (2008) included Sierra del Toro conglomerate as part of the Magallanes basin axial channel-belt. This study recognizes that outcrops on Sierra del Toro include at least three major conglomeratic units, each of which is interpreted to represent a submarine channel-complex within the axial channel-belt. The thicknesses of these channel complexes range from 20 to 300 m, and the widths range from less than 1 km to greater than 5 km (Fig. 2A, inset). From oldest to youngest, they are named the "Condor", "Guanaco," and "Wildcat" complexes (Fig. 2). These channel complexes are composed largely of conglomerate

and sandstone and are separated by mudstone. The undifferentiated channel fill that overlies the Wildcat complex (Fig. 2) is also conglomeratic, but recent erosion and scree cover prevent the discrimination of channel morphologies or the genetic association with other complexes.

The Condor complex consists of three westward-migrating, offset stacked submarine channels (Fig. 2) and was named and described by Barton et al. (2007) and O'Byrne et al. (2007). The conglomeratic channel fill commonly contains dune and bar forms (O'Byrne et al. 2007). Jobe et al. (2009a) showed that paleocurrents were directed to the southeast and the orientation of the eastern margin of the Condor complex is 165° (Fig. 2). The Guanaco complex (Figs. 2A, B) contains at least five individual channels, each 5-70 m thick and 0.1-1 km wide. These channels stack quasi-aggradationally, centered above the eastern margin of the Condor complex and underneath the western margin of the Wildcat complex (Fig. 2). The Guanaco complex is exposed only on the north side of Sierra del Toro (Fig. 2). Jobe et al. (2009b) speculate that the overlying Wildcat complex may downcut to the south, and amalgamate the two complexes, thereby rendering them indistinguishable on the south side of Sierra del Toro.

**Wildcat Channel Complex.---**The uppermost channel complex on Sierra del Toro is named the "Wildcat channel complex" because of the rare wildcat *Oncifelis geofforyi* ("gato montés" in Chilean Spanish) that resides among the conglomerate outcrops.

This complex forms the caprock of Sierra del Toro (Fig. 2) and exhibits average and maximum thicknesses of 143 and 294 m, respectively. The Wildcat complex is 3.5 km wide and is exposed for 6 km downdip; with the average thickness of 143 m, there are ~ 3 $km^3$ of Wildcat channel fill on Sierra del Toro. Paleocurrent indicators from the Wildcat complex indicate average (mean ± 1σ) paleoflow to the southeast (153 ± 40°; Fig. 2A at upper right), consistent with map trends of the channel margins (Fig. 2A). Previous work on the Wildcat channel complex is limited to two studies. Hubbard et al. (2007) described the "Sarmiento Vista" (SV) locale on the northern face of Sierra del Toro (Fig. 2B), where amalgamated, conglomeratic channel-fill onlaps the eastern margin. Jobe et al. (2009c) incorporated the Sarmiento Vista locale into an examination of the entire eastern margin of the Wildcat complex.

**Dataset and Methods.---**A total of 18 measured sections logged at 10 cm resolution, totaling over 2000 m, provide the basis for correlation and analysis of the Wildcat complex. These are supplemented by 975 paleocurrent measurements, facies mapping, and photopanel interpretation. Facies proportions were calculated by dividing the thickness of each facies in a measured section by the total thickness of that section, normalized for covered intervals. Amalgamation ratio (AR), defined as the number of amalgamation surfaces divided by the total number of sedimentation units (Manzocchi et al. 2007; Romans et al. 2009a), was also calculated for each measured

section. In order to measure the erosive power of turbidity currents, only conglomerate, sandstone, and mudstone units were used to compute AR; debris flows and slurry flows were not incorporated because they represent either hybrid flows or nonturbulent flows. Five ash beds were sampled from below, within, and above the Wildcat complex, and their locations are marked on subsequent figures; these ashes are being dated by A. Bernhardt (unpublished data).

## LITHOFACIES OF THE WILDCAT CHANNEL COMPLEX

Lithofacies of the Wildcat channel complex generally display evidence of rapid deposition by energetic sediment gravity flows. Table 1 provides specific descriptive characteristics of each lithofacies. Hubbard et al. (2008) provide a thorough description and motivation for the use of the lithofacies scheme for the Cerro Toro Formation (Fig. 3 and Table 1 in Hubbard et al. 2008), and this study adapts their terminology with some modifications germane to the Wildcat complex. Lithofacies continuity from Sierra del Toro to the Cordillera Manuel Señoret, more than 50 km downflow, suggests that the Cerro Toro axial channel-belt was an immense and continuous depositional system. The term "mudstone" is used throughout this study as a generic term describing a sedimentary rock composed of silt and clay where specific amounts of each constituent are not specified and no process of sedimentation is implied (adapted from Bates and Jackson 1984).

*IIIscg – Clast-Supported Conglomerate*

IIIscg consists of clast-supported, normally graded and imbricated, sand-matrix cobble conglomerate (Fig. 3A). Basal contacts with IIIm commonly show large "canoe" flutes (Fig. 3B). Where IIIscg overlies IIIss, large (1-2 m high) flame structures are frequently developed.

*IIIsf – Slurry-Flow Conglomerate*

IIIsf sedimentation units can be up to 40 m thick, but are commonly 4-11 m thick and display an upward transformation from a basal clast-supported conglomerate to an upper conglomeratic mudstone (Fig. 3C). The clast-supported basal divisions typically occupy < 25% of the total unit thickness, and the transition can be gradual or abrupt. Basal contacts often display flute casts and load structures (Fig. 3C). Extrabasinal clasts range in size from sand to boulders (Fig. 3D), but cobbles are predominant. Units of IIIsf show normal grading of extrabasinal clasts (Fig. 3D), while large (up to 6 m) intrabasinal clasts (i.e., raft blocks) are concentrated near the top of the upper matrix-supported division (Fig. 3C). Deep burrows of the *Glossifungites* ichnofacies have also been recognized in IIIsf (Hubbard and Shultz 2008).

The sedimentation mechanics of these units remain poorly understood, even after extensive study (Scott 1966; Winn and Dott 1979; Sohn et al. 2002; Crane 2004;

Hubbard et al. 2008). Flute casts indicate turbulent flow behavior, whereas matrix-supported divisions indicate cohesive debris-flow-like behavior. Consequently, these rheologically complex flows are best termed slurry flows (*sensu* Lowe and Guy 2000; Crane 2004), where both cohesive and turbulent forces are active during deposition and complex temporal and/or spatial (head to tail) changes in rheology are likely (Fisher 1983; Sohn et al. 2002). A synonymous term for slurry flow is "hybrid sediment gravity flow" (Haughton et al. 2009). These conglomeratic slurry flow units, although common in the Cerro Toro Formation, seem to be quite rare in the rock record; the closest analog seems to be units from the Proterozoic of Ontario that are interpreted by Miall (1985) as submarine "clast-rich debris flows."

With much focus on flow rheology, plausible triggering mechanisms for IIIsf have not been fully discussed. Two possible scenarios are envisioned here: the first, which Hubbard et al. (2008) prefer, is a conglomeratic turbidity current (i.e., IIIscg) that erodes and incorporates enough muddy intrabasinal material during downslope movement to change its rheology. Alternatively, IIIsf could be created by large-scale submarine slope failures, where interbedded conglomerate, sandstone, and mudstone are mixed and variably disaggregated during downslope movement. We prefer this mechanism since the high initial sediment concentration in a flow generated by slope failure facilitates the incorporation of large intrabasinal clasts into the flow rather than

the flow having to erode the clasts piecemeal. Furthermore, intrabasinal clasts are rare in IIIscg, suggesting that they are not frequently eroded.

### *IIIsf – Debris-Flow Conglomerate*

IIIdf deposits, unlike IIIsf, do not have clast supported bases; rather, IIIdf is composed completely of matrix-supported conglomeratic mudstone. Individual sedimentation units are commonly 2-4 m thick and contain randomly dispersed extrabasinal and intrabasinal clasts (cf. upper division in Fig. 3C). IIIdf are much more common in the western part of the Wildcat complex.

### *IIIss – Thick-Bedded, Amalgamated Sandstone*

IIIss consists predominantly of structureless (Fig. 3E) or dish-structured (Fig. 3F) medium-grained sandstone that is often amalgamated. Granule and pebble lags (Fig. 3F) are commonly found at amalgamation surfaces, suggesting that a significant amount of sediment bypassed this proximal part of the axial channel-belt.

### *IIIsm – Interbedded Sandstone and Mudstone*

IIIsm units are commonly ~ 1 m thick, consisting of interbedded traction-structured sandstone (Fig. 3G) and moderately bioturbated mudstone (Fig. 3G). IIIsm can also contain thin beds of conglomerate, usually as local lenses. IIIsm in the channel

fill is more common in the western part of the Wildcat complex, and out-of-channel IIIsm exists in notable quantity adjacent to the eastern margin.

### *IIIm – Mudstone with Thin Sandstone Interbeds*

These layered, rhythmic, laminated to thin-bedded mudstone units make up the bulk of the Cerro Toro Formation (Fig. 3H), but make up only 2% (in thickness) of the Wildcat channel fill. Thin-bedded sandstone is sparse, composing about 10-20% of IIIm (Fig. 3H).

## ASYMMETRY OF THE WILDCAT CHANNEL COMPLEX

### *Units 1, 2, 3, 4, and 5 and Their Lateral Facies Changes*

Vertical changes in lithofacies stacking patterns and accompanying stratigraphic surfaces were used to package the Wildcat channel complex into the five units mapped in the outcrops. Each unit is distinct in terms of facies and architecture, and each records a discrete phase in channel evolution. These units, from oldest to youngest, are (Figs. 4A, 4B): Unit 1, Unit 2, Unit 3, Unit 4, and Unit 5. These units are hierarchically similar to the fourth-order packaging of Hubbard et al. (2008) and probably represent individual channels within the Wildcat complex. These units are equivalent in hierarchy to the "channel elements" of Pyles et al. (2010). Each unit in the Wildcat channel complex displays an across-channel westward decrease in amalgamation ratio

and the proportion of conglomeratic and amalgamated facies (Figs. 4A, 4B, 5). Bed-thickness plots do not show any lateral trends that are statistically significant, signifying that amalgamation and facies proportions are the distinguishing characteristics of the Wildcat facies asymmetry. The eastern side of the Wildcat complex consists of highly amalgamated lithofacies onlapping an architecturally simple, steep (averaging 9.4°) margin. The character of the Wildcat channel fill drastically changes westward (Fig. 4A) and is characterized by: (1) the westward *decrease* in proportion of IIIscg, IIIss, and IIIsf (Figs. 4, 5); (2) the westward *increase* in proportion of IIIsm and IIIdf (Figs. 4, 5); and (3) the westward *decrease* in AR (Fig. 4 inset graphs). The western margin of the Wildcat complex is shallow (averaging 7.1°), heterolithic, and composite, with many internal surfaces and drapes (Fig. 4). These changes are enumerated below for both the north-side and south-side exposures on Sierra del Toro.

### *North-Side Exposures of the Wildcat Channel Complex*

**Eastern Margin: North-Side Exposure.---**Nine measured sections (Table 2) document the complete eastern margin of the Wildcat channel complex on the north side of Sierra del Toro (Fig. 4A). Over an across-channel distance of 1.2 km, more than 200 m of channel fill onlaps and pinches out against the margin, resulting in a margin slope of 9.4°. Figure 6 shows the Sarmiento Vista locale, where 100 m of highly amalgamated (AR = 0.93; Fig. 4A inset), predominantly conglomeratic channel fill onlap

the margin surface that is cut into IIIm (Fig. 4A). About 50 m of the onlap occurs between the measured sections SV2 and SV1, where the lowest IIIdf and Unit 1, composed of IIIscg and IIIss, pinch out (Fig. 6). The lowest IIIdf may be a localized slump near the stepped channel margin (Figs. 4A, 6). Unit 2, composed predominantly of IIIsf and about 45 m thick, pinches out abruptly just east of SV1 (Figs. 4A, 6A). Near the eastern margin, Unit 3 consists of IIIscg and IIIss whereas Unit 4 consists of IIIss (Fig. 6). At the Flame section, Units 3 and 4 pinch out against the margin (Figs. 3C, 4A, 7A). Unit 5, composed of IIIscg and local IIIss, pinches out just east of the WC section (Figs. 4A, 7C), and the abandonment of the channel is marked by onlapping IIIsm documented in the CZM sections (Figs. 4A, 7B). The average slope of the eastern margin surface is 9.4° (Fig. 4A), although it is uneven and locally exceeds 15° (Figs. 4A, 6A). This margin resembles the southwestern margin of the Paine complex in the Silla Syncline (Crane and Lowe 2008) as well as the western margin of the axial channel-belt farther south at Cerro Mocho (Hubbard et al. 2008).

A 40-m-thick accumulation of IIIsm is present outside the channel adjacent to Unit 5 at the uppermost eastern margin (section CZM1 in Figs. 4A, 7B). This accumulation may represent a levee deposited by flows overbanking the channel at its eastern margin and flowing down the regional southeast slope. Decompaction of the surrounding IIIm would elevate the IIIsm overbank accumulation above the conglomeratic channel fill even more, supporting a levee interpretation. However,

lateral exposure is limited and therefore no unambiguous conclusions about the genetic relationship between the IIIsm overbank accumulation and the Wildcat channel fill are possible.

**Wildcat Facies Transition: North-Side Exposure.---**The westward facies changes on the north side of Sierra del Toro are shown in Figure 8, where amalgamated IIIscg, IIIss, and IIIscg/ss at Sarmiento Vista and ETF pass westward into bedded IIIsm and IIIdf at the WTF section. Amalgamation ratio (AR) along this transect decreases from 0.93 to 0.62 (Fig. 4A inset), representing the addition of interbedded mudstone as IIIsm becomes the dominant facies. Each of the units making up the Wildcat complex demonstrate these facies changes (Fig. 5). Unit 1 shows a distinct change from IIIscg and IIIss to IIIsm (Figs. 5, 8). In Unit 2, IIIsf decreases sharply in proportion and is replaced by IIIdf and IIIsm (Figs. 4A, 5, 8). Unit 3 thickens to the west due to the addition of IIIsm at the expense of IIIscg and IIIss (Figs. 4A, 5, 8). Unit 4, IIIss in the east, becomes much less amalgamated and more heterolithic to the west (Figs. 4A inset, 5). Unit 5 is well exposed in the CC section, where it is much less amalgamated (Fig. 4A inset) than in eastern sections. This westward change is manifested in Figure 5 by the sharp drop in the percentage of IIIscg and IIIsf as well as a 35% increase in IIIsm. The eastern margin of the underlying Guanaco channel complex is also exposed in this locale (Fig. 8) and consists of many individual channel fills, composed predominantly of

IIIscg and IIIsf, onlapping out-of-channel IIIm. The Guanaco complex can be traced to the south into the CC section (Figs. 2, 9).

**Western Margin: North-Side Exposure.---**Outcrops of the western margin are well exposed at two locations on the north side of Sierra del Toro (Figs. 8, 9). Just west of the WTF section, more than 30 m of Unit 1 onlaps the western margin (Fig. 8). At WTF, Unit 1 is not amalgamated (AR = 0.62; inset of Fig. 4A) and consists of almost 50% IIIsm (Fig. 5). The western margin is also exposed 2.2 km downdip of WTF at the CC section (Figs. 2A, 9), where Units 1-5 are bedded, laterally discontinuous, and exhibit an AR of 0.70 (Fig. 4A inset). Units 1, 2, and 3, constituting over 85 m of heterolithic, non-amalgamated channel fill, lap out onto at least three internal surfaces that collectively form the composite western margin of the Wildcat channel complex (Fig. 9A). A predominance of IIIsm and IIIdf in Units 2 and 3 attests to the muddy, fine-grained nature of the margin (Fig. 5). Scree cover and a post-depositional thrust fault (Figs. 2, 9) preclude the exposure of the onlap of Units 4 and 5 onto the western margin. However, these units are clearly exposed on the south side (see below). The Wildcat western margin closely resembles the northern margin of the Paine complex in the Silla Syncline (Crane and Lowe 2008). The underlying Guanaco channel complex shows margin architecture similar to the Wildcat near the CC section (Fig. 9B), where IIIscg, IIIsm, and IIIsf display multiple pinchout surfaces against the western margin (Fig. 9B).

*South-Side Exposures of the Wildcat Channel Complex*

Units 1-5 are traceable from the north-side exposures to the south side of Sierra del Toro and allow the three-dimensional (3D) characterization of the Wildcat channel complex. Due to cliffy exposures, only three measured sections document the Wildcat complex on the south side (Fig. 4B). However, outcrop photomosaics demonstrate that, as on the north side, the south-side exposures of the Wildcat channel complex display marked lateral changes in amalgamation ratio (inset of Fig. 4B) and facies proportions (Fig. 5), and the eastern and western margin architectures considerably differ.

**Eastern Margin: South-Side Exposure.---**The south-side exposure of the eastern margin records the onlap of 110 m of channel fill over a distance of 680 m, resulting in a margin slope of 9.1°, similar to that in the northern exposure. The AR of the south-side exposure of the eastern Wildcat channel fill is quite high (0.90; Fig 4B inset) and Units 3-5 appear massive and conglomeratic in outcrop (Fig. 7D). Units 1 and 2, near the eastern margin, are poorly exposed (Figs. 2C, 7D), but probably onlap the eastern margin just west of the H2O section. Unit 3, composed of IIIscg and IIIss, and Unit 4, composed of IIIss, pinch out progressively onto the eastern margin just east of the H2O section (Figs. 4B, 7D). Unit 5, composed of IIIscg, continues to the east, pinching out east of the SSM section (Figs. 2C, 4B).

**Wildcat Facies Transition: South-Side Exposure.---**The westward facies changes in the Wildcat complex are also well exposed on the south side of Sierra del Toro at the "Rocas" locale (Fig. 10). The Rocas section (Fig. 4B) represents a point midway in this transition, where facies proportions are similar to the ETF section on the north side of Sierra del Toro (Figs. 2, 4A, 5). Just northwest of the Rocas section, Unit 1 changes from IIIscg and IIIss to IIIsm and Unit 2 changes from IIIsf to IIIsm and IIIdf (Figs. 4B, 10). The IIIscg and IIIss of Unit 3 and the IIIss of Unit 4 also show the facies transition westward into IIIsm (Figs. 4B, 10). These facies changes are characterized at the bed scale by the progressive thinning and loss of IIIscg into IIIss, which is replaced by IIIsm (inset of Fig. 10). Unit 5 remains conglomeratic at this locale (Fig. 10), but eventually thins and fines to the west (Fig. 11). The lowest IIIsf unit (Figs. 4B, 10, 11) may be part of the Guanaco complex, but exact correlation from the north side is not possible due to scree cover.

**Western Margin: South-Side Exposure.---**The final pinchout of the western margin of the Wildcat channel complex is fully exposed on the south side of Sierra del Toro (Fig. 11). Unlike the eastern margin, the western margin is *not* a steep, amalgamated, single surface. Rather, the western margin is composite and consists of multiple erosional surfaces, some of which are draped. The onlap of 200 m of channel

fill over 1.6 km results in a non-decompacted margin angle of 7.1°, which is shallower than that of the eastern margin. Not all beds terminate against the basal margin surface (Figs. 4B, 11): Units 1 and 2 seem to onlap the basal margin surface, whereas Units 3-5 pinch out onto multiple internal surfaces. The last occurrence of IIIscg on the western side is about 400 m from the final pinchout, and IIIsm continues until the final pinchout of the western margin (Fig. 11). This contrasts the eastern margin, where IIIscg directly abuts IIIm at the final pinchout (Fig. 7). Beneath and adjacent to the western-margin surface, the out-of-channel mudstone, IIIm, contains no overbank IIIsm accumulation similar to that at the eastern margin (cf. Fig. 7).

## DISCUSSION

### *Meander-Bend Architecture of the Cerro Toro Axial Channel-Belt*

The axial channel-belt of the Cerro Toro Formation displays very low (1.06) sinuosity (Fig. 1; Hubbard et al. 2008). The exposure at Sierra del Toro allows for the detailed analysis of a single right-hand meander bend in the axial channel-belt (orange dashed line in Fig. 2A). Evidence in the Wildcat channel complex for this low-sinuosity meander bend includes: (1) the facies asymmetry and distribution; (2) the modest architectural asymmetry; (3) the contrasting morphology and stratigraphic architecture of the margins; and (4) the sandy overbank accumulation that is found adjacent to the amalgamated and steep (eastern) margin. The amalgamated, thick-bedded,

conglomeratic facies and the steep, simple margin in the eastern Wildcat form the outer bank of the meander bend, complete with a sandy (IIIsm) overbank accumulation adjacent to Unit 5 (Figs. 4A, 5, 6, 7). In the western Wildcat, the thin-bedded, non-amalgamated, fine-grained facies (Figs. 4, 5), the shallow, composite margin with many internal onlap surfaces (Figs. 9, 11), and the absence of sandy overbank facies (Figs. 9, 11) are most consistent with deposition on the inner bend of a meandering channel. The Puchkirchen axial channel-belt in the Molasse basin of Austria forms a notable analog for the very low sinuosity and channel architecture seen in the Wildcat (cf. Hubbard et al. 2009).

**Differing Margin Architecture and Facies of the Wildcat Channel Complex.---** Although locally exceeding 15°, the outer (eastern) bank of the Wildcat channel complex has an average angle of 9.4°, whereas that of the inner (western) bank is 7.1°. The modest architectural asymmetry is attributed in part to the low sinuosity of the axial channel-belt, inasmuch as higher sinuosity submarine channels have been shown to have greater architectural asymmetry (Pirmez and Flood 1995; Babonneau et al. 2002; Antobreh and Krastel 2006; Pyles et al 2010). The packaging of the Wildcat complex into Units 1-5 suggests multiple episodes of channel incision and filling, but the morphology and preservation of the resultant surfaces and internal margins differs significantly at the eastern and western margins. It is likely that due to centrifugal

effects and elevated shear stress, currents preferentially eroded the eastern outer bank and deposited amalgamated coarse-grained facies, leading to its steep, conglomeratic, amalgamated nature (Figs. 4, 6, 7). The stepped nature of the eastern margin (Fig. 6) probably represents margins of individual units; however, severe amalgamation has rendered these multiple surfaces into a single, steep, stepped outer bank. The IIIsm overbank sandstone accumulation adjacent to the outer bend of the Wildcat complex (Figs. 4A, 7) likely represents the deposits of turbidity currents that experienced flow stripping (*sensu* Piper and Normark 1983) around the outer bend of the Wildcat channel complex. Although a levee accumulation is expected in the overbank of the outer bend (cf. Posamentier 2003) and levees have been identified elsewhere in the axial channel-belt (Hubbard et al. 2008), no definitive levee geometries are apparent on Sierra del Toro (Fig. 7).

Flows interacted differently with the inner bend, where lower shear stress resulted in the fine-grained and non-amalgamated nature of the western margin (Figs. 4, 5). The lack of large-scale erosion and amalgamation during the multiple incision and fill episodes of Units 1-5 led to the preservation of each unit's margin, resulting in a heterolithic, complicated, composite western margin (Figs. 4, 9, 11). This style of inner-bank architecture has also been documented in modern sinuous submarine channels (Antobreh and Krastel 2006). The conglomeratic basal region of flows did not reach the western margin, resulting in the in-channel deposition of IIIsm near the margin. Since

these IIIsm deposits occur within the confines of the channel fill, they may represent inner-levee deposits (cf. Hubbard et al. 2008).

**Lack of Lateral Accretion Deposits.---**The architectural and facies asymmetry in the Wildcat channel complex agree with models of normal helical circulation within sinuous submarine channels (Johannesson and Parker 1989; Abreu et al. 2003; Pirmez and Imran 2003; Straub et al. 2008); "reverse" helical flow (Keevil et al. 2006; Keevil et al. 2007; Peakall et al. 2007) is not supported by the observed facies data in this study. Lateral accretion deposits (Abreu et al. 2003; Arnott 2007; Dykstra and Kneller 2009; Pyles et al. 2010) are expected in sinuous submarine channels with normal helical flow. However, no lateral accretion deposits are observed in the Wildcat channel complex, suggesting that there was no migration of the channel or erosion of the banks during deposition. The IIIm that composes the banks may have been compacted and cohesive, resisting major bank erosion and lateral migration. Alternatively, the Wildcat complex may have been entrenched and aggradational due to levee growth, a commonly documented stage in the evolution of submarine channels (Clark and Pickering 1996; Peakall et al. 2000; Kolla et al. 2007). In the Magallanes basin, levee confinement may have been a factor, but the higher-order confinement of the axial channel-belt by the foredeep probably was the driving factor for preventing the development of sinuosity and lateral accretion (cf. Hubbard et al. 2005; Hubbard et al. 2008; Hubbard et al. 2009).

The structurally-induced prevention of sinuosity has also been documented on the modern seafloor (Clark and Cartwright 2009). The Wildcat channelform was probably cut by highly erosive flows, setting up the very low-sinuosity meandering profile. The channelform was then filled in an aggradational manner, with multiple episodes of incision and filling (Units 1-5 in Figs. 4, 9, 11) without significant lateral migration of the channel. The abandonment phase is represented in the Wildcat complex by the thin IIIsm package that overlies the conglomeratic channel fill (Figs. 4A, 7B).

### *Paleoflow Patterns in the Wildcat Channel Complex: Loss of Confinement and Consequent Overbank Deposition*

The dominant paleoflow direction in the Cerro Toro axial channel-belt is to the south-southeast (Scott 1966; Winn and Dott 1979; Hubbard et al. 2008). The Guanaco complex and thin-bedded turbidites beneath the Wildcat complex also display south-southeast-directed paleoflows, down the inferred regional slope of the axial channel-belt (Fig. 2A). In the Wildcat complex, south-southeastward paleoflow patterns are consistent across the channelform in Units 1 (155° ± 20° in the format mean ± 1$\sigma$), 2 (157° ± 17°) and 3 (164° ± 15 °) (Fig. 12). In Units 4 and 5, however, paleoflow directions are not unidirectional, but exhibit divergence across the channel. In Unit 4, paleoflow was 162° ± 42° in the east and 225° ± 10° in the west (Fig. 12). In Unit 5, paleoflow was 121° ± 23° in the east and 230° ± 7° in the west (Fig. 12).

Consistent south-southeastward paleoflow in Units 1-3 indicate that the flows were fully confined within the channel. This inference is supported by the lack of sandy overbank accumulations adjacent to Units 1, 2, and 3 (Fig. 4). Diverging paleoflow directions in Units 4 and 5 of the Wildcat channel fill are thought to reflect the gradual loss of confinement as the channel filled and flows were able to overtop the banks. Currents flowing through the Wildcat channel complex during deposition of Units 4 and 5 were not fully confined and consequently spread out within the channel and spilled out of the channel along the outer bank (Fig. 12). The sandy overbank accumulation on the outer bank adjacent to Unit 5 (Figs. 4A, 7B) displays southeast paleoflow directions (Fig. 12), indicating that the flows, once outside the channel, moved down the regional basin slope. The undifferentiated channel fill lying above and to the west of the Wildcat complex shows southwestward paleoflow (Fig 2A) and may represent the continuation of this spillover that eventually resulted in channel avulsion. However, exposure is limited in the undifferentiated unit (Fig. 2A), and no unambiguous conclusions about the genetic relationship between it and the Wildcat complex are possible.

### *Predictive Depositional Model of Sinuous, Asymmetric Submarine Channels*

Studies of sinuous submarine channels (e.g., Kneller 1995; Peakall et al. 2000) generally focus on channel morphology and spatial evolution, but relatively few have

provided details of internal facies distributions and architecture, which are essential for numerical and experimental models (Zeng and Lowe 1997; Imran et al. 1999; Peakall et al. 2007; Straub et al. 2008). The few studies providing facies data on sinuous submarine channel fill (Campion et al. 2000; Hickson and Lowe 2002) lack the full set of data concerning internal variations in grain size, facies, and amalgamation crucial for input into numerical or more generalized models of channel evolution. This study provides this detailed internal facies data for a very well exposed, large-scale channel complex. Furthermore, the Wildcat complex is a natural system, eliminating problems of scaling common to numerical and experimental models.

Figure 13 is a generalized summary of the Wildcat channel complex that incorporates the observed architectural and facies asymmetry and meander bend architecture discussed above. The schematic model shows a theoretical flow traversing the channel and depositing amalgamated, coarse-grained channel-fill facies and sandy overbank deposits adjacent to a steep erosional margin that forms the outer bend of the channel (Fig. 13). These features contrast with the thinner-bedded, low net-to-gross channel-fill facies and muddy overbank deposits adjacent to a shallow, composite margin along the inner bend (Fig. 13). Due to the very low sinuosity, the channel shows modest architectural asymmetry at the bends (A-A', C-C' of Fig. 13), and is probably symmetric in straight reaches and near inflection points (B-B' of Fig. 13). Hydraulic considerations and the observed differences in channel geometry and internal fill in

sinuous fluvial channels (Leopold and Wolman 1960) and submarine channels (Campion et al. 2000; Pyles et al. 2010) suggest that the key elements of this observational model of the Wildcat channel complex have applicability in predicting the general facies distributions and channel geometries in other sinuous submarine channels, especially where exposures are poor or only seismic data is available. For higher-sinuosity channels, the architectural and facies asymmetry should be even more pronounced than for low-sinuosity channels; unfortunately, quantifying the correlation between asymmetry and sinuosity is not possible at this time due to the limited data available. Finally, this model (Fig. 13) can also be used to amend numerical and flume models, which commonly build highly sinuous channels with symmetric cross-sections, even at bend apices (Keevil et al. 2006; Keevil et al. 2007; Straub et al. 2008).

*Possible Presence of Knickpoints in the Axial Channel-Belt at Sierra del Toro*

The three-dimensional exposure at Sierra del Toro allows the construction of a correlation panel down depositional dip (Fig. 14A). This panel demonstrates a major change in the downdip architecture of the axial channel-belt involving: (1) the north-to-south increase in bed thickness (Fig. 14A) and amalgamation ratio (Fig. 14B) of the Wildcat complex; (2) more than 80 m of downcutting of the undifferentiated channel fill into the uppermost Wildcat complex (Fig. 14A); (3) the downdip "disappearance" of the Guanaco channel complex (Figs. 2, 14A; Jobe et al. 2009b) and inferred downcutting of

the Wildcat complex; (4) the lower elevation of the base of the Wildcat complex on the south side of Sierra del Toro (Fig. 2); and (5) southward-dipping faults (Fig. 14C) in out-of-channel IIIm on the east side of Sierra del Toro. The local deep and abrupt downcutting suggests that that there may have been a knickpoint in the axial channel-belt coincident with the present location of Sierra del Toro. Knickpoints commonly cause drastic downslope changes in submarine-channel architecture (Mitchell 2006; Heiniö and Davies 2007; Toniolo and Cantelli 2007) similar to those observed in the Wildcat channel complex.

Three scenarios are possible for the formation of a knickpoint in the axial channel-belt at Sierra del Toro. The first is a deep-seated north-south-trending rift graben inherited from Late Jurassic back-arc extension of the predecessor Rocas Verdes basin (Fig. 1D; Biddle et al. 1986; Fildani and Hessler 2005). Subsurface seismic reflection data indicate the presence of such a graben 20 km downdip (Fosdick et al. 2009) that may extend northward and tip out underneath Sierra del Toro. These grabens potentially were still undergoing thermal subsidence during Cerro Toro deposition and may have caused a steepening downslope gradient under Sierra del Toro. The channel architecture expected by this first scenario may be similar to that shown by Heiniö and Davies (2007). The second scenario is a knickpoint caused by the downstream confluence of the axial channel-belt and the Silla Syncline tributary system postulated by Crane and Lowe (2008) and Hubbard et al. (2008). The sediment added to

the system at this confluence may have generated enhanced local erosion, leading to the formation of a knickpoint that then migrated upstream in the axial channel-belt to Sierra del Toro. The third scenario is a knickpoint created by a southward-dipping ("down-to-the-basin") growth-fault system. The presence of southward-dipping growth faults and associated mini-basin fill have been demonstrated in overlying Tres Pasos deposits just 5 km east of Sierra del Toro (Shultz and Hubbard 2005). Furthermore, Figure 14C demonstrates the presence of southward-dipping normal faults on the east side of Sierra del Toro that presumably continue west beneath the Wildcat channel complex. These faults, if syndepositional, would have resulted in the formation of a knickpoint, perhaps similar in geometry to that documented on the modern seafloor (Adeogba et al. 2005).

### *Application to Hydrocarbon Exploration*

Facies asymmetry in submarine channels (Stelting et al. 1985a; Stelting et al. 1985b; Campion et al. 2000) can provide significant barriers or baffles to fluid flow in reservoirs within submarine channel fill. Exposures of the Wildcat complex show that across a "reservoir/full field scale" channel fill, significant changes in facies and AR occur within and between Units 1-5 (Figs. 4, 13). These lateral facies changes may severely impact vertical and horizontal permeability across a similar reservoir. Most of these facies variations are small enough to lie below seismic resolution, which would

result in poor facies prediction and unexpected borehole results. Furthermore, these facies changes take place over a distance of about 1 km (Figs. 4A, 5), a much smaller distance than typical deep-water well spacing. The differing margin architecture documented here also has implications for reservoir heterogeneity: the amalgamated, steep, outer-bank margin contains many units that provide quality reservoir facies, but the complicated, heterolithic nature of the inner-bank fill not only indicates low-quality reservoir facies but also the presence of severe baffles and barriers for fluid flow in a petroleum reservoir. The data and depositional model presented here can aid in formulating development strategies in reservoirs within sinuous submarine channels. Also, the facies data presented in this study can provide input for more quantitative reservoir models of asymmetric submarine channel fill rather than the simple models currently in use that commonly depict homogeneous channel fill (Labourdette, 2007; Sweet and Sumpter, 2007).

## CONCLUSIONS

The 3.5 km wide, 300 m thick Wildcat channel complex on Sierra del Toro represents the proximal portion of the axial channel-belt of the Upper Cretaceous Cerro Toro Formation in the Magallanes retro-arc foreland basin, Chile. The Wildcat complex displays strong facies asymmetry and modest cross-sectional, or architectural asymmetry. Paleocurrent patterns within the channel complex and the geometry of its

margins indicate that the axial channel-belt in this locale had a very low sinuosity and was characterized by flows moving to the south-southeast. The Wildcat complex is interpreted to represent part of a gentle right-hand meander bend of the axial channel-belt. Around this bend the channel was characterized by a simple, erosional outer bank and a heterogeneous, composite inner bank. Outer-bend facies are highly amalgamated, conglomeratic, and thick-bedded while inner-bend facies are sandy/muddy, thin-bedded, and not amalgamated. A sandy overbank accumulation exists only adjacent to the outer bend. Turbidity currents flowing through the axial channel-belt responded to the low sinuosity by preferentially depositing coarse sediment in the outer bend as well as in the overbank due to flow momentum and centrifugal forces. The lack of lateral accretion deposits indicates that the channel belt was entrenched and not migrating laterally. The early evolution of the channel fill was characterized by flows that were fully confined by the channel. During the late stage of channel evolution, flow directions became divergent towards the margins, suggesting that flows were beginning to spill outside of the channel, an inference supported by the overbank sandstone accumulation along the outer bend.

The observed facies and cross-sectional asymmetry in the Wildcat complex probably characterize the fill of most sinuous submarine channels, and greater facies and cross-sectional asymmetry is expected with higher sinuosity channels. This asymmetry can result in highly compartmentalized reservoirs and therefore needs to be

incorporated into subsurface models. Furthermore, the abundant data concerning channel asymmetry presented here can be used to refine flume experiments and numerical models of sinuous submarine channel evolution.

## ACKNOWLEDGMENTS

We would like to thank foremost the member companies of the **S**tanford **P**roject **O**n **D**eepwater **D**epositional **S**ystems (**SPODDS**) industrial affiliates program for funding this field research and ZRJ's graduate research at Stanford University. These companies include or have included Aera, Anadarko, Chevron, ConocoPhillips, Devon, ENI-AGIP, ExxonMobil, Hess, Marathon, Nexen, Occidental, PetroBras, Reliance, Rohöl-Aufsuchungs AG (R.A.G.), and Shell. The Department of Geological and Environmental Sciences at Stanford University also provides additional financial support through fellowships and teaching assistantships. The field work would not have been possible without the benevolence and generosity of the landowners of Sierra del Toro: Jorge Portales Iglesias of the Mirador del Payne resort and "Don" Arturo Kroeger of Cerro Guido. Southern Chile is a cold, windy field locale, and Dominic Armitage, Julie Fosdick, and Lisa Stright deserve special thanks for enduring. Steve Hubbard deserves gratitude for initiating research on Sierra del Toro. This study has profited from insightful discussions with Dominic Armitage, Steve Graham, Bill Morris, Kirt Campion, Zoltan Sylvester, and many other SPODDS affiliates. Finally, we are

especially appreciative of the direction and lucidity provided by the reviewers David Pyles, Rufus Brunt, and Bill McCaffrey.

REFERENCES

Abreu, V., Sullivan, M., Pirmez, C., and Mohrig, D., 2003, Lateral accretion packages (LAPs): an important reservoir element in deep water sinuous channels: Marine and Petroleum Geology, v. 20, p. 631-648.

Adeogba, A.A., McHargue, T.R., and Graham, S.A., 2005, Transient fan architecture and depositional controls from near-surface 3-D seismic data, Niger Delta continental slope: American Association of Petroleum Geologists, Bulletin, v. 89, p. 627-643.

Antobreh, A., and Krastel, S., 2006, Morphology, seismic characteristics and development of Cap Timiris Canyon, offshore Mauritania: a newly discovered canyon preserved-off a major arid climatic region: Marine and Petroleum Geology, v. 23, no. 1, p. 37-59.

Armitage, D.A., Romans, B.W., Covault, J.A., and Graham, S.A., 2009, The influence of mass-transport-deposit surface topography on the evolution of turbidite architecture: The Sierra Contreras, Tres Pasos Formation (Cretaceous), Southern Chile: Journal of Sedimentary Research, v. 79, no. 5, p. 287-301.

Arnott, R.W.C., 2007, Stratal architecture and origin of lateral accretion deposits (LADs) and conterminuous inner-bank levee deposits in a base-of-slope sinuous channel, lower Isaac Formation (Neoproterozoic), East-Central British Columbia, Canada: Marine and Petroluem Geology, v. 24, p. 515-528.

Babonneau, N., Savoye, B., Cremer, M., and Klein, B., 2002, Morphology and architecture of the present canyon and channel system of the Zaire deep-sea fan: Marine and Petroleum Geology, v. 19, no. 4, p. 445-467.

Barton, M.D., Steffens, G.S., and O'Byrne, C.J., 2007, Facies architecture of a submarine-slope channel complex, Condor West channel, Cerro Toro Formation, Chile, *in* Nilsen, T., Shew, R., Steffens, G., and Studlick, J., eds., Atlas of Deep-Water Outcrops: American Association of Petroleum Geologists, Studies in Geology 56, p. 149-153.

Bates, R.L., and Jackson, J.A., 1984, Dictionary of Geological Terms: Third Edition: New York, Anchor Books, 571 p.

Bernhardt, A., Jobe, Z.R., and Lowe, D.R., 2008, The evolution of an elongate foreland basin: The deep- to shallow-marine filling of the Cretaceous Magallanes basin, Chile, *in* Schofield, K., Rosen, N.C., Pfeiffer, D., and Johnson, S., eds., Answering the Challenges of Production from Deep-water Reservoirs: Analogues and Case Histories to aid a New Generation: SEPM, Gulf Coast Section (GCS), 28th Annual Research Conference, p. 268-310.

Bernhardt, A., Jobe, Z.R., and Lowe, D.R., in press, Stratigraphic evolution of a deep-water slope channel-lobe complex system in a narrow trough within the Magallanes foreland basin, southern Chile, Marine and Petroleum Geology, doi:10.1016/j.marpetgeo.2010.05.013

Biddle, K.T., Uliana, M.A., Mitchum, R.M., Fitzgerald, M.G., and Wright, R.C., 1986, The stratigraphic and structural evolution of the central and eastern Magallanes Basin, southern South America, in Allen, P.A., and Homewood, P., eds., Foreland basins: International Association of Sedimentologists, Special Publication 8, p. 41-61.

Bouma, A.H., 1962, Sedimentology of Some Flysch Deposits: A Graphic Approach to Facies Interpretation: Amsterdam, Elsevier, 168 p.

Buffington, E.C., 1952, Submarine "Natural Levees": Journal of Geology, v. 60, no. 5, p. 473-479.

Campion, K.M., Sprague, A.R., Mohrig, D., Lovell, R.W., Drzewiecki, P.A., Sullivan, M.D., Ardill, J.A., Jensen, G.N., and Sickafoose, D.K., 2000, Outcrop expression of confined channel complexes, *in* Weimer, P., Slatt, R.M., Coleman, J., Rosen, N.C., Nelson, H., Bouma, A.H., Styzen, M.J., and Lawrence, D.T., eds., Deep-Water Reservoirs of the World: SEPM, Gulf Coast Section (GCS), 20th Annual Research Conference, p. 127-150.

Clark, J.D., and K.T. Pickering, 1996, Architectural elements and growth patterns of submarine channels: applications to hydrocarbon exploration: American Association of Petroleum Geologists, Bulletin, v. 80, p. 194-221.

Clark, I.R., and Cartwright, J.A., 2009, Interactions between submarine channel systems and deformation in deepwater fold belts: Examples from the Levant Basin, Eastern Mediterranean sea: Marine and Petroleum Geology, v. 26, no. 8, p. 1465-1482.

Covault, J.A., Romans, B.W., and Graham, S.A., 2009, Outcrop expression of a continental-margin-scale shelf-edge delta from the Cretaceous Magallanes Basin, Chile: Journal of Sedimentary Research, v. 79, no. 7, p. 523-539.

Crane, W.H., 2004, Depositional history of the Upper Cretaceous Cerro Toro Formation, Silla Syncline, Magallanes Basin, Chile: Ph.D. dissertation, Stanford University, Stanford, California, 275 p.

Crane, W.H., and Lowe, D.R., 2008, Architecture and evolution of the Paine channel complex, Cerro Toro Formation (Upper Cretaceous), Silla Syncline, Magallanes Basin, Chile: Sedimentology, v. 55, no. 4, p. 979-1009.

Dalziel, I.W., de Wit, M.J., and Palmer, K.F., 1974, Fossil marginal basin in the southern Andes: Nature, v.

250, p. 291-294.

De Ruig, M.J., and Hubbard, S.M., 2006, Seismic facies and reservoir characteristics of a deep-marine channel belt in the Molasse foreland basin, Puchkirchen Formation, Austria: American Association of Petroleum Geologists, Bulletin, v. 90, no. 5, p. 735-752.

Deptuck, M.E., Steffens, G.S., Barton, M., and Pirmez, C., 2003, Architecture and evolution of upper fan channel-belts on the Niger Delta slope and in the Arabian Sea: Marine and Petroleum Geology, v. 20, no. 6-8, p. 649-676.

Dodov, B., and Foufoula-Georgiou, E., 2004, Generalized hydraulic geometry: Insights based on fluvial instability analysis and a physical model: Water Resources Research, v. 40, W12201, 15 p.

Dott, R.H., Winn, R.D. and Smith, C.H.L., 1982, Relationship of Late Mesozoic and Early Cenozoic sedimentation to the tectonic evolution of the southernmost Andes and Scotia arc, *in* Craddock, C., ed., Antarctic Geoscience, University of Wisconsin Press, Madison, p. 193-202.

Dykstra, M., and Kneller, B., 2009, Lateral accretion in a deep-marine channel complex: implications for channellized flow processes in turbidity currents: Sedimentology, v. 56, no. 5, p. 1411-1432.

Fildani, A., Cope, T.D., Graham, S.A., and Wooden, J.L., 2003, Initiation of the Magallanes foreland basin: Timing of the southernmost Patagonian Andes orogeny revised by detrital zircon provenance analysis: Geology, v. 31, no. 12, p. 1081-1084.

Fildani, A., and Hessler, A.M., 2005, Stratigraphic record across a retroarc basin inversion: Rocas Verdes-Magallanes basin, Patagonian Andes, Chile: Geological Society of America, Bulletin, v. 117, no. 11-12, p. 1596-1614.

Fildani, A., Romans, B.W., Fosdick, J.C., Crane, W.H., and Hubbard, S.M., 2008, Orogenesis of the Patagonian Andes as reflected by basin evolution in southernmost South America, *in* Spencer, J.E., and Titley, S.R., eds., Ores and Orogenesis: Circum-Pacific Tectonics, Geologic Evolution, and Ore Deposits: Arizona Geological Society, Digest, v. 22, p. 259-268.

Fisher, R.V., 1983, Flow transformations in sediment gravity flows: Geology, v. 11, p. 273-274.

Flood, R.D., and Damuth, J.E., 1987, Quantitative characteristics of sinuous distributary channels on the Amazon deep-sea fan: Geological Society of America, Bulletin, v. 98, no. 6, p. 728-738.

Fosdick, J.C., Romans, B.W., Fildani, A., Calderón, M., Bernhardt, A., and Graham, S.A., 2009, Shortening under extended circumstances: regional structure of the Cretaceous-Neogene Patagonian fold-thrust belt and Magallanes Basin, Chile and Argentina (51° 30' S) (abstract), GSA Annual

Meeting, Program with Abstracts.

Hampton, M.A., 1975, Competence of Fine-grained Debris Flows: Journal of Sedimentary Petrology, v. 45, no. 4, p. 834-844.

Haughton, P., Davis, C., McCaffrey, W., and Barker, S., 2009, Hybrid sediment gravity flow deposits - classification, origin and significance: Marine and Petroleum Geology, v. 26, no. 10, p. 1900-1918.

Hauthal, R., 1907, Croquis geológico de la región entre el Lago Argentino y el Seno Ultima Esperanza, 1/500000: Ber. Naturf. Gesell. Freiburg i.Br., v. 15, pl. 1.

Hay, A.E., Murray, J.W., and Burling, R.W., 1983a, Submarine channels in Rupert Inlet, British Columbia: I: Morphology: Sedimentary Geology, v. 36, p. 289-315.

Hay, A.E., Murray, J.W., and Burling, R.W., 1983b, Submarine channels in Rupert Inlet, British Columbia: II. Sediments and sedimentary structures: Sedimentary Geology, v. 36, p. 317-339.

Hay, A.E., 1987a, Turbidity currents and submarine channel formation in Rupert Inlet, British Columbia: 1. Surge observations: Journal of Geophysical Research, v. 92, no. C3, p. 2875-2881.

Hay, A.E., 1987b, Turbidity currents and submarine channel formation in Rupert Inlet, British Columbia 2. The roles of continuous and surge type flow: Journal of Geophysical Research, v. 92, no. C3, p. 2883-2900.

Heiniö, P., and Davies, R.J., 2007, Knickpoint migration in submarine channels in response to fold growth, western Niger Delta: Marine and Petroleum Geology, v. 24, no. 6-9, p. 434-449.

Hickson, T.A., and Lowe, D.R., 2002, Facies architecture of a submarine fan channel-levee complex: the Juniper Ridge Conglomerate, Coalinga, California: Sedimentology, v. 49, no. 2, p. 335-362.

Hubbard, S.M., de Ruig, M.J. and Graham, S.A., 2005, Utilizing outcrop analogs to improve subsurface mapping of natural gas-bearing strata in the Puchkirchen Formation, Molasse Basin, Upper Austria: Austrian Journal of Earth Sciences, v. 98, p. 52-66.

Hubbard, S.M., Romans, B.W., Erohina, T., and Lowe, D.R., 2007, Facies and internal architecture of deep-water channel fill in the Cerro Toro Formation, Sarmiento Vista, Chile, *in* Nilsen, T., Shew, R., Steffens, G., and Studlick, J., eds., Atlas of Deep-Water Outcrops: American Association of Petroleum Geologists, Studies in Geology 56, p. 140-142.

Hubbard, S.M., and Shultz, M.R., 2008, Deep burrows in submarine fan-channel deposits of the Cerro Toro Formation (Cretaceous), Chilean Patagonia: Implications for firmground development and

colonization in the deep sea: Palaios, v. 23, no. 4, p. 223-232.

Hubbard, S.M., Romans, B.R., and Graham, S.A., 2008, Deep-water foreland basin deposits of the Cerro Toro Formation, Magallanes basin, Chile: architectural elements of a sinuous basin axial channel belt: Sedimentology, v. 55, no. 5, p. 1333-1359.

Hubbard, S.M., de Ruig, M.J., and Graham, S.A., 2009, Confined channel-levee complex development in an elongate depo-center: Deep-water Tertiary strata of the Austrian Molasse basin: Marine and Petroleum Geology, v. 26, no. 1, p. 85-112.

Hubbard, S.M., Fildani, A., Romans, B.W., Covault, J.A., and McHargue, T.R., 2010, High-relief slope clinoform development: Insights from outcrop, Magallanes basin, Chile: Journal of Sedimentary Research, v. 80, no. 5, p. 357-375.

Imran, J., Parker, G., and Pirmez, C., 1999, A nonlinear model of flow in meandering submarine and subaerial channels: Journal of Fluid Mechanics, v. 400, p. 295-331.

Jobe, Z.R., Bernhardt, A., Fosdick, J.C., and Lowe, D.R., 2009a, Cerro Toro channel margins on Sierra del Toro, *in* Fildani, A., Hubbard, S.M., and Romans, B.R., eds., Stratigraphic Evolution of Deep-Water Architecture: Examples of Controls and Depositional Styles from the Magallanes Basin, Southern Chile: SEPM, Field Trip Guidebook no. 10, p. 31-34.

Jobe, Z.R., Bernhardt, A., and Lowe, D.R., 2009b, Downdip "disappearance" of the Guanaco channel complex: Amalgamation by downcutting due to gradient steepening, *in* Fildani, A., Hubbard, S.M., and Romans, B.R., eds., Stratigraphic Evolution of Deep-Water Architecture: Examples of Controls and Depositional Styles from the Magallanes Basin, Southern Chile: (abstract) SEPM, Field Trip Guidebook no. 10, p. 52-53.

Jobe, Z.R., Bernhardt, A., Hubbard, S.M., and Lowe, D.R., 2009c, Wildcat channel complex axis-to-margin architecture, Sierra del Toro, *in* Fildani, A., Hubbard, S.M., and Romans, B.R., eds., Stratigraphic Evolution of Deep-Water Architecture: Examples of Controls and Depositional Styles from the Magallanes Basin, Southern Chile: SEPM, Field Trip Guidebook no. 10, p. 35-38.

Johannesson, H., and Parker, G., 1989, Linear theory of river meanders, *in* Ikeda, S. and Parker, G., eds., River Meandering: American Geophysical Union, Water Resources Monograph, no. 12 p. 181-212.

Johnson, J.E., Paull, C.K., Normark, W.R., and Ussler, W., 2009, The Monterey fan channel turbidite record offshore central California: (abstract) Insights into submarine canyon processes: 83rd Annual Pacific Section AAPG - SEPM - SEG Convention, Ventura, California, May 2-6, 2009.

Katz, H.R., 1963, Revision of Cretaceous stratigraphy in Patagonian Cordillera of Ultima Esperanza,

Magallanes Province, Chile: American Association of Petroleum Geologists, Bulletin, v. 47, p. 506-524.

Keevil, G.M., Peakall, J., Best, J.L., and Amos, K.J., 2006, Flow structure in sinuous submarine channels: Velocity and turbulence structure of an experimental submarine channel: Marine Geology, v. 229, p. 241-257.

Keevil, G.M., Peakall, J., and Best, J.L., 2007, The influence of scale, slope and channel geometry on the flow dynamics of submarine channels: Marine and Petroleum Geology, v. 24, p. 487-503.

Klaucke, I., Hesse, R., and Ryan, W.B., 1998, Morphology and structure of a distal submarine trunk channel: The Northwest Atlantic Mid-Ocean Channel between lat 53° N and 44° 30' N: Geological Society of America, Bulletin, v. 110, no. 1, p. 22-34.

Kneller, B.C., 1995, Beyond the turbidite paradigm: physical models for deposition of turbidites and their implications for reservoir prediction, *in* Hartley, A., and Prosser, D.J., eds., Characterization of Deep Marine Clastic Systems: Geological Society of London, Special Publication 94, p. 29-46.

Kolla, V., Bourges, P., Urruty, J.M., and Safa, P., 2001, Evolution of deep-water Tertiary sinuous channels offshore Angola (west Africa) and implications for reservoir architecture: American Association of Petroleum Geologists, Bulletin, v. 85, no. 8, p. 1373-1405.

Kolla, V., Posamentier, H.W., and Wood, L.J., 2007, Deep-water and fluvial sinuous channels—Characteristics, similarities and dissimilarities, and modes of formation: Marine and Petroleum Geology, v. 24, no. 6-9, p. 388-405.

Labourdette, R., 2007, Integrated three-dimensional modeling approach of stacked turbidite channels: American Association of Petroleum Geologists, Bulletin, v. 91, no. 11, p. 1603-1618.

Lamb, M.P., Parsons, J.D., Mullenbach, B.L., Finlayson, D.P., Orange, D.L., and Nittrouer, C.A., 2008, Evidence for superelevation, channel incision, and formation of cyclic steps by turbidity currents in Eel Canyon, California: Geological Society of America, Bulletin, v. 120, no. 3-4, p. 463-475.

LaPointe, M.F., and Carson, M.A., 1986, Migration patterns of an asymmetric meandering river: The Rouge River, Quebec: Water Resources Research, v. 22, no. 5, p. 731-743.

Leopold, L.B., and Wolman, M., 1960, River meanders: Geological Society of America, Bulletin, v. 71, no. 6, p. 769-793.

Lowe, D.R., 1982, Sediment gravity flows: II. Depositional models with special reference to the deposits of high-density turbidity currents: Journal of Sedimentary Petrology, v. 52, no. 1, p. 279-297.

Lowe D.R. and Guy, M., 2000, Slurry-flow deposits in the Britannia Formation (Lower Cretaceous), North Sea: a new perspective on the turbidity current and debris flow problem: Sedimentology, v. 47, no. 1, p. 31-70.

Macellari, C.E., Barrio, C.A., and Manassero, M.J., 1989, Upper Cretaceous to Paleocene depositional sequences and sandstone petrography of southwestern Patagonia (Argentina and Chile): Journal of South American Earth Sciences, v. 2, no. 3, p. 223-239.

Manzocchi, T., Walsh, J.J., Tomasso, M., Strand, J., Childs, C., and Haughton, P.D.W., 2007, Static and dynamic connectivity in bed-scale models of faulted and unfaulted turbidites, *in* Jolley. S.J., Barr, D., Walsh, J.J., and Knife, R.J., Structurally Complex Reservoirs: Geological Society of London, Special Publication 292, p. 309-336.

Melton, F.A., 1936, An empirical classification of flood-plain streams: Geographical Review, v. 26, no. 4, p. 593-609.

Menard, H.W., 1955, Deep-sea channels, topography, and sedimentation: American Association of Petroleum Geologists, Bulletin, v. 39, no. 2, p. 236-255.

Miall, A.D., 1985, Sedimentation on an early Proterozoic continental margin under glacial influence: the Gowganda Formation (Huronian), Elliot Lake area, Ontario, Canada: Sedimentology, v. 32, no. 6, p. 763-788.

Miall, A.D., 1996, The Geology of Fluvial Deposits; Sedimentary Facies, Basin Analysis, and Petroleum Geology: Berlin, Springer, 582 p.

Mitchell, N.C., 2006, Morphologies of knickpoints in submarine canyons: Geological Society of America, Bulletin, v. 118, no. 5, p. 589-605.

Nanson, G.C., 1980, Point bar and floodplain formation of the meandering Beatton River, northeastern British Columbia, Canada: Sedimentology, v. 27, p. 3-29.

Natland, M.L., González, E., Cañón, A., and Ernst, M., 1974, A System of Stages for Correlation of Magallanes Basin Sediments: Geological Society of America, Memoir 139, 126 p.

O'Byrne, C.J., Prather, B.E., Pirmez, C.E., Barton, M.D., and Steffens, G.S., 2007, Coarse-grained bar forms in the Condor Channel Complex, Cerro Toro Formation at Lago Sarmiento, Chile, *in* Nilsen, T., Shew, R., Steffens, G., and Studlick, J., eds., Atlas of Deep-Water Outcrops: American Association of Petroleum Geologists, Studies in Geology 56, p. 154-156.

Peakall, J., McCaffrey, B., and Kneller, B., 2000, A process model for the evolution, morphology, and architecture of sinuous submarine channels: Journal of Sedimentary Research, v. 70, no. 3, p. 434-448.

Peakall, J., Amos, K.J., Keevil, G.M., William Bradbury, P., and Gupta, S., 2007, Flow processes and sedimentation in submarine channel bends: Marine and Petroleum Geology, v. 24, no. 6-9, p. 470-486.

Piper, D.J.W., and Normark, W.R., 1983, Turbidite depositional patterns and flow characteristics, Navy submarine fan, California borderland: Sedimentology, v. 30, p. 681-694.

Pirmez, C., and Flood, R.D., 1995, Morphology and structure of Amazon Channel: Proceedings of the Ocean Drilling Program. Part A, Initial Report, v. 155, p. 23-45.

Pirmez, C., and Imran, J., 2003, Reconstruction of turbidity currents in Amazon Channel: Marine and Petroleum Geology, v. 20, no. 6-8, p. 823-849.

Posamentier, H.W., 2003, Depositional elements associated with a basin floor channel-levee system: case study from the Gulf of Mexico: Marine and Petroleum Geology, v. 20, no. 6-8, p. 677-690.

Pyles, D.R., Jennette, D.C., Tomasso, M., Beaubouef, R.T., and Rossen, C., 2010, Concepts learned from a 3D outcrop of a sinuous slope channel complex: Beacon Channel Complex, Brushy Canyon Formation, West Texas: Journal of Sedimentary Research, v. 80, no. 1, p. 67-96.

Romans, B.W., Hubbard, S.M., and Graham, S.A., 2009a, Stratigraphic evolution of an outcropping continental slope system, Tres Pasos Formation at Cerro Divisadero, Chile: Sedimentology, v. 56, p. 737-764.

Romans, B.W., Fildani, A., Graham, S.A., Hubbard, S.M., and Covault, J.A., 2009b, Importance of predecessor basin history on the sedimentary fill of a retroarc foreland basin: provenance analysis of the Cretaceous Magallanes basin, Chile (50-52° S): Basin Research, doi:10.1111/j.1365-2117.2009.00443.x

Satur, N., Kelling, G., Cronin, B.T., Hurst, A., and Gürbüz, K., 2005, Sedimentary architecture of a canyon-style fairway feeding a deep-water clastic system, the Miocene Cingöz Formation, southern Turkey: significance for reservoir characterisation and modelling: Sedimentary Geology, v. 173, no. 1-4, p. 91-119.

Scott, K.M., 1966, Sedimentology and dispersal pattern of a Cretaceous flysch sequence, Patagonian Andes, southern Chile: American Association of Petroleum Geologists, Bulletin, v. 50, no. 1, p. 72-107.

Shultz, M.R., Fildani, A., Cope, T.D., and Graham, S. A., 2005, Deposition and stratigraphic architecture of an outcropping ancient slope system: Tres Pasos Formation, Magallanes Basin, southern Chile, *in* Hodgson, M., and Flint, S., Submarine Slope Systems: Processes and Products: Geological Society of London Special Publication 244, p. 27-50.

Shultz, M.R., and Hubbard, S.M., 2005, Sedimentology, stratigraphic architecture, and ichnology of gravity-flow deposits partially ponded in a growth-fault-controlled slope minibasin, Tres Pasos Formation (Cretaceous), Southern Chile: Journal of Sedimentary Research, v. 75, no. 3, p. 440-453.

Sohn, Y.K., Choe, M.Y., and Jo, H. R., 2002, Transition from debris flow to hyperconcentrated flow in a submarine channel (the Cretaceous Cerro Toro Formation, southern Chile): Terra Nova, v. 14, no. 5, p. 405-415.

Stelting, C.E., and DSDP Leg 96 Shipboard Scientists, 1985a, Migratory characteristics of a mid-fan meander belt, Mississippi Fan, *in* Bouma, A.H., Barnes, N.E., and Normark, W.R., eds., Submarine Fans and Related Turbidite Sequences: New York, Springer-Verlag, p. 283-290.

Stelting, C.E., Pickering, K.T., Bouma, A.H., Coleman, J.M., Cremer, M., Droz, L., Meyer-Wright, A.A., Normark, W.R., O'Connell, S., Stow, D.A.V., and DSDP Leg 96 Shipboard Scientists, 1985b, Drilling results on the Middle Mississippi Fan, *in* Bouma, A.H., Barnes, N.E., and Normark, W.R., eds., Submarine Fans and Related Turbidite Sequences: New York, Springer-Verlag, p. 275-282.

Straub, K.M., Mohrig, D., McElroy, B., Buttles, J., and Pirmez, C., 2008, Interactions between turbidity currents and topography in aggrading sinuous submarine channels: A laboratory study: Geological Society of America, Bulletin, v. 120, no. 3-4, p. 368-385.

Sweet, M.L., and Sumpter, L.T., 2007, Genesis field, Gulf of Mexico: Recognizing reservoir compartments on geologic and production time scales in deep-water reservoirs: American Association of Petroleum Geologists, Bulletin, v. 91, no. 12, p. 1701-1729.

Toniolo, H., and Cantelli, A., 2007, Experiments on upstream-migrating submarine knickpoints: Journal of Sedimentary Research, v. 77, no. 9, p. 772-783.

Valenzuela, A.A.S., 2006, Proveniencia sedimentaria de los estratos de Cabo Nariz y Formación Cerro Toro, Cretacico Tardio-Paleoceno, Magallanes, Chile: Ph.D. Dissertation, Universidad de Chile, Santiago, 153 p.

Wilson, T.J., 1991, Transition from back-arc to foreland basin development in the southernmost Andes: Stratigraphic record from the Ultima Esperanza District, Chile: Geological Society of America, Bulletin, v. 103, no. 1, p. 98-111.

Winn, R.D., and Dott, R.H., 1977, Large-scale traction-produced structures in deep-water fan-channel conglomerates in southern Chile: Geology, v. 5, no. 1, p. 41-44.

Winn, R.D., and Dott, R.H., 1979, Deep-water fan-channel conglomerates of Late Cretaceous age, southern Chile: Sedimentology, v. 26, no. 2, p. 203-228.

Yu, H., Chiang, C., and Shen, S., 2009, Tectonically active sediment dispersal system in SW Taiwan margin with emphasis on the Gaoping (Kaoping) Submarine Canyon: Journal of Marine Systems, v. 76, no. 4, p. 369-382.

Zeil, W., 1958, Sedimentation in der Magallanes-Geosynklinale mit besonderer Berücksichtigung des Flysch: Geologische Rundschau, v. 47, p. 425-443.

Zeng, J., and Lowe, D.R., 1997, Numerical simulation of turbidity current flow and sedimentation: I. Theory: Sedimentology, v. 44, p. 67-84.

Table 1. Characterization of lithofacies in the Wildcat channel complex, Cerro Toro Formation, exposed on Sierra del Toro.

Table 2. Characterization and AR (amalgamation ratio) of the 19 stratigraphic sections measured at Sierra del Toro.

Figure 1. Overview of the Magallanes retro-arc foreland basin, located in southern Chile. A) Paleogeographic map of the Magallanes basin during deposition of the Cerro Toro Formation (Campanian). Inset map shows location of the Magallanes basin in South America. Main transport was basin-axial and directed southward, parallel to the advancing thrust front. Black box denotes location of Part B; D-D□ denotes the location of Part D. Map modified from Hubbard et al. (2008). B) Landsat image, courtesy of NASA MRSID. Solid red outlines show the modern extent of Cerro Toro conglomeratic channel-fill deposits. Black box denotes the location of Fig. 2A. C) Stratigraphy of the Magallanes basin, compiled from Natland et al. (1974), Wilson (1991), Fildani et al. (2003), Romans et al. (2009b). This section does not represent true thickness; the Cerro Toro Formation is ~ 2000 m thick in the northern Magallanes basin. D) Schematic cross section of the Magallanes basin during deposition of the Cerro Toro Formation in the foredeep of the basin, modified from Fildani et al. (2003). Location of cross section is shown in Part A.

Figure 2. The location of Sierra del Toro in the northern Magallanes basin. A) The study area of Sierra del Toro, displaying the eastward stacking of channel-fill deposits where flow was directed to the southeast (153°). Inset shows the > 1000 m of stratigraphy exposed on Sierra del Toro. The Wildcat channel complex is 3.5 km wide and exposed for 7 km in the downdip direction. The orange dashed line is the inferred planform of the Wildcat complex. Fifteen sections were measured in the Wildcat complex; their locations and average paleoflow directions are shown on the map. The undifferentiated channel fill lies above the Wildcat complex, but limited exposure prevents determination of its genetic relationship with the Wildcat. The legend details colors for sections (green) and faults (yellow) that are used consistently in all figures. B, C) Outcrop photos showing Sierra del Toro and the Wildcat channel complex. Colors of dashed lines correspond to Part A and the black triangle shows tie between photos. B) The north side of

Sierra del Toro, displaying all three channel complexes stacking progressively eastward. C) The south side of Sierra del Toro. Notice the Wildcat channel-fill deposits thinning onto both the eastern and western margins. The eastern margin of the Condor can be seen; however, the Guanaco is not present on the south side of Sierra del Toro.

Figure 3. Lithofacies of the Wildcat channel complex, Cerro Toro Formation. Refer to Table 1 for more information. (A, B) Clast-supported conglomerate (IIIscg). A) Normal grading and clast imbrication (white triangles). Field book is 20 cm tall. B) Large "canoe" flutes eroded into underlying IIIm mudstone. Note southward paleoflow. C, D) Slurry-flow conglomerate (IIIsf) at the Flame section (see Fig. 2 for location). C) A typical slurry-flow sedimentation unit, with the base loaded into the underlying IIIss. The inset photo is a zoom-in of the sedimentation unit – note the clast-supported base and the matrix-supported top with large raft blocks of IIIss (probably derived from the underlying bed). Geologist for scale. D) The extremely coarse-grained nature of the clast-supported divisions of IIIsf, where boulders can reach > 40 cm. Jacob's-staff divisions are 10 cm. E, F) Thick-bedded, amalgamated sandstone (IIIss). E) Multiple IIIss sedimentation units, where concretions are developed along amalgamation surfaces. Geologist for scale. F) Dish structures are frequently developed in IIIss. The inclined amalgamation surface is lined by a cross-stratified gravelly lag. G) Interbedded sandstone and mudstone (IIIsm) within the channel fill, showing traction structures and *Skolithos* ichnofacies bioturbation. Also interbedded is a local conglomerate lens, which is slightly erosional. These local conglomerates are sometimes developed in IIIsm. Pen at left is 15 cm long. H) Mudstone with thin sandstone interbeds (IIIm). This package of out-of-channel IIIm is over 1000 m thick and N:G is ~ 10% (see Fig. 14C). Geologist for scale. Inset photos top and bottom show the thin sandstone interbeds and the *Skolithos* ichnofacies bioturbation in IIIm, respectively. Pen is 13 cm long.

Figure 4. Depositional-strike correlation panels of the Wildcat channel complex (see Fig. 2 for location). Paleoflow is into the page for both panels. A) North-side correlation panel, displaying 12 measured sections across 3.5 km of channel fill that document the evolution of Units 1-5. The eastern margin is steep (9.4°) and onlapped by amalgamated, conglomeratic facies. A facies change occurs to the west, and the western Wildcat consists of thin-bedded, less amalgamated

facies such as IIIsm and IIIdf. B) South-side correlation panel, displaying three measured sections across 3.5 km of channel fill. The eastern and western margins of the Wildcat are exposed on the south side (Figs. 2, 7, 12), and the facies change is drastic from east to west.

Figure 5. Lithofacies-proportion transects across the north-side exposures of the Wildcat channel complex. The facies change in the Wildcat complex is demonstrated by the westward decrease in the amalgamation ratio and the proportion of conglomeratic facies. Units 1-5 all show this drastic facies change laterally in the channel fill.

Figure 6. The eastern, amalgamated side of the Wildcat channel complex (north-side exposure). White and red dashed lines indicate the margin surface and the unit boundaries, respectively. A) Outcrop photo of the eastern side, demonstrating the onlap of more than 100 m of channel fill (white dashed line is the margin surface). Paleoflow is into the page and obliquely to the right. In the background of the photo, the rest of the channel fill onlaps the margin surface (see Fig. 7). Arrows at upper left denote the perspective of photos in Figure 7. B) Outcrop photo of the amalgamated facies (AR = 0.90) of the eastern side of the Wildcat. Inset shows geologist for scale; more than 200 m of channel fill are exposed on this outcrop face. Fourth-order Units 1, 2, 3, 4, and 5 are discussed throughout the text. Units 3, 4, and 5 can be correlated to those seen in Figure 7C, D.

Figure 7. Eastern margin of the Wildcat channel complex on Sierra del Toro (north-side and south-side exposures). A) View to south that shows the rapid thinning of over 100 m of channel fill (foreground) onto the margin surface. Paleoflow is obliquely to the right and into the page. Dashed box shows location of Part B; see Part C for perspective location. B) The easternmost channel-fill and overbank deposits of the Wildcat complex; location provided in Part A. Unit 5 (IIIscg) pinches out just east of CZM5, and the IIIsm abandonment fill pinches out just to the east. Note the IIIsm overbank accumulation measured in CZM1 that lies adjacent to Unit 5, the uppermost channel fill. C) Looking onto the northern exposure of the eastern margin, where Units 4 and 5 onlap. Note the perspective location of Part A and the location of Fig. 6 around the corner. D) The southern exposure of the eastern margin, where Units 3, 4, and 5 onlap the

margin from left to right (i.e., west to east). Note the highly amalgamated nature of this exposure.

Figure 8. Facies transition in the central Wildcat (north-side exposure). Inset shows location of photo on the north side of Sierra del Toro. From measured section ETF to WTF, amalgamation decreases from 0.80 to 0.62 and the proportion of IIIss and IIIscg decreases by 22% (Fig. 5). This lateral facies change is also expressed by a decrease in cliffy exposures. The Guanaco channel complex is also present in this locale, and it pinches out to the east and west. Thrust faulting is focused at this locale, probably due to loss of structural rigidity caused by the facies transition.

Figure 9. Western margin of the Wildcat complex (north-side exposure). A) The complicated margin architecture that characterizes the western margin as well as the westward bed thinning and loss of conglomerate. Units 1, 2, and 3 transition here into IIIsm and then into out of channel mudstone (IIIm). Unfortunately, a fault and scree obscures the pinchout of Units 4 and 5; however, those are clearly exposed on the south side (see Fig. 12). Inset shows location of Part B. B) Close-up view of the western margin; see Part A for location of photo. Note the geologist for scale. The complicated margin architecture is demonstrated by both the Wildcat and Guanaco complexes.

Figure 10. Facies transition in the central Wildcat (south-side exposure). Units 1 and 2 are already IIIsm here, whereas Units 3 and 4 transition here to IIIsm (see inset). Unit 5 changes facies from IIIscg to IIIsm just to the west (see Fig. 12). Note the loss of conglomerate and loss of amalgamation from east to west.

Figure 11. Western margin of the Wildcat complex (south-side exposure). White dashed lines mark the margins and bed tracings, and red lines are unit boundaries. A) Looking north, Units 1-5 thin and fine to the west (left) and are replaced by IIIsm and finally by out-of-channel mudstone (IIIm). Note the last occurrence of IIIscg in the western Wildcat. Black box denotes the location of the inset photo, which shows IIIsm thinning onto the margin. B) Looking south,

the amalgamated central part of the Wildcat can be seen in the background, where the Rocas section was measured. The complicated margin architecture is apparent here, with multiple onlap surfaces corresponding to the unit boundaries. The dramatic facies change from east to west is evident from this vantage point.

Figure 12. Evolution of paleoflow in the Wildcat channel complex.
Paleoflow below the Wildcat as well as in Units 1, 2, and 3 are southeastward, consistent with regional indicators. However, Units 4 and 5 document a spreading of paleoflow, indicating a loss of confinement. This is especially apparent in Unit 5, where the east and west sides show a spread of 144°. Adjacent to the fanning paleoflow in Unit 5 is the IIIsm overbank accumulation, indicating that it was sourced from inside the channel by Unit 5 flows. The southeastward paleoflow indicators in the overbank represent the flows responding to regional paleoslope after exiting confinement. All paleoflow averages shown are mean ± 1σ; geometry is based on Figure 4A.

Figure 13. Data-based depositional model of sinuous, asymmetric submarine channels.
The model incorporates data from this study and predicts facies distributions throughout the reach of the channel. Note the difference in margin angle between the inner and outer bends. Overbank accumulations of sandstone are restricted to the outer bend due to flow stripping and loss of confinement in the late stages of evolution. Bed thickness, conglomerate proportion, and AR decrease from the outer bend to the inner bend due to changing flow properties. This model can be used to predict and constrain facies distributions in outcrops, subsurface data, flume experiments, and numerical models.

Figure 14. Correlation panel demonstrating the downdip architectural changes of the Wildcat channel complex, perhaps due to the presence of an intrachannel knickpoint. A) Correlation panel showing the observed downcutting of the undifferentiated channel fill above the Wildcat as well as the inferred downcutting of the base of the Wildcat complex from north to south. These downcutting events are interpreted to be knickpoints in the channel belt responding to a gradient steepening. This steepening is likely due to the presence of N-S rift grabens inherited from the predecessor basin. B) Amalgamation ratio (AR) transect down depositional dip, showing that

the increase in both indices corresponds with the presence of the knickpoints. C) Photo of the eastern flank of Sierra del Toro (see inset map in Part A for location) that demonstrates the presence of southward-dipping normal faults that may extend to the west beneath the channel fill. These faults may be syndepositional and related to an intrachannel knickpoint that is responsible for the downdip changes in architecture of the Wildcat channel complex.

| Lithofacies | Characteristic grain size | Sedimentary structures and depositional processes (R & S divisions from Lowe 1982; T divisions from Bouma 1962) | Average / maximum sedimentation unit thickness | Secondary and notable features | Percentage (by thickness) of Wildcat channel fill<br>Average amalgamation ratio (AR) |
|---|---|---|---|---|---|
| **IIIscg**<br>Clast-supported conglomerate | Cobbles:<br>12 x 6 cm average<br>40 x 25 cm max<br>Medium sand matrix<br>Local IIIss lenses | Normallly graded ($R_1$), imbricated and/or crudely planar laminated ($R_3$); high-density turbidity currents (Lowe 1982) | 1.7 m / 6 m | Intrabasinal clasts; flute casts; cross bedding; sand-filled scours; large (~ 1m) flame structures | 41%<br>0.95 |
| **IIIsf**<br>Slurry-flow conglomerate | Basal divison: clast-supported cobbles with sandy and muddy matrix<br>Upper division: poorly sorted muddy matrix with sand, gravel, & raft blocks | Normally graded (both clasts and matrix);"'slurry flows" (Lowe and Guy 2000) or "hybrid sediment gravity flows" (Haughton et al. 2009) | 4-11 m / 40 m | Flute casts and flame structures; Large (> 5 m) intrabasinal raft blocks common in upper divisions | 14%<br>0.85 |
| **IIIdf**<br>Debris-flow conglomerate | Mudstone matrix with sand and gravel clasts | Random grain dispersion and orientation; debris flow (Hampton 1975) | 2-4 m / 14 m | Dispersed intrabasinal raft blocks | 7%<br>N/A |
| **IIIss**<br>Thick-bedded, amalgamated sandstone | Medium-grained (66%) to coarse-grained (28%) sand; common gravel lags and IIIscg lenses | Structureless, normally graded, dish structured, flame structured ($S_2$/$T_a$); high-density turbidity currents(Lowe 1982) | 0.5-1 m / 5 m | Fe-bearing concretions up to 1 m diameter; flute casts; traction-structured tops ($T_{bc}$); cross-stratification ($S_1$, $T_t$) rare | 24%<br>0.80 |
| **IIIsm**<br>Interbedded sandstone and mudstone | Fine-grained sand interbedded with mudstone; gravel lags and conglomerate lenses are rarely developed | Planar-laminated ($T_b$) and ripple-laminated ($T_c$); low-density turbidity currents (Bouma, 1962) | 30 cm / 100 cm sandstone<br>5 cm / 25 cm mudstone | Flute casts; bioturbation by *Skolithos* & *Zoophycus* ichnofacies; convolute lamination and water-escape structures; | 12%<br>0.50 |
| **IIIm**<br>Mudstone with thin sandstone interbeds | Mudstone = silt+clay; fine- to medium-grained sandstone | Planar-laminated mud ($T_d$) ripple-laminated sand ($T_c$); low-density turbidity currents (Bouma, 1962) | 2 cm avg mudstone 5 / 50 cm sandstone<br>IIIm - 22/200 cm avg/max in channel; >1000 m out-of-channel | Bioturbation by *Skolithos* ichnofacies; Fe-bearing carbonate concretions in both mud and sand; *Inoceramus* body fossils | 2%<br>0.20 |

| Section abbrev. | Measured section name | Side of Sierra del Toro | Thickness (m) | Wildcat channel-fill thickness (m) | Average thickness of IIIscg / IIIss | Average thickness of IIIsm / IIIm | Amalgamation Ratio (AR) | Average flow direction / # of indicators | Notes |
|---|---|---|---|---|---|---|---|---|---|
| CZM1 | Chorrillo Zapata Margin 1 | North | 29 | 0 | N/A | 210 / 24 cm | 0.48 | **167°** / 16 | Overbank IIIsm accumulation at E margin |
| CZM2 | Chorrillo Zapata Margin 2 | North | 12 | 0 | N/A | 120 30 | 0.50 | **106°** / 8 | Channel abandonment IIIsm facies at E margin |
| CZM3 | Chorrillo Zapata Margin 3 | North | 16 | 0 | N/A | 78 29 | 0.45 | -- | Channel abandonment IIIsm facies at E margin |
| CZM4 | Chorrillo Zapata Margin 4 | North | 26 | 0 | N/A | 86 21 | 0.47 | **162°** / 12 | Channel abandonment IIIsm facies at E margin |
| CZM5 | Chorrillo Zapata Margin 5 | North | 40 | 3 | 2 m / 40 cm | 140 29 | 0.52 | **168°** / 45 | Channel abandonment IIIsm facies at E margin |
| WC | Wildcat Thrust | North | 70 | 32 | 88 / 90 cm | 1.2 / 0.25 m | 0.73 | -- | Channel fill & abandonment IIIsm facies at E margin |
| Flame | Flame | North | 105 | 105 | 3.2 m / 94 cm | 63 13 | 0.76 | **086°** / 66 | Amalgamated eastern side of the Wildcat |
| SV1 | Sarmiento Vista 1 | North | 147 | 147 | 170 / 90 cm | N/A / 43 | 0.93 | **127°** / 54 | Amalgamated eastern side of the Wildcat |
| SV2 | Sarmiento Vista 2 | North | 197 | 197 | 95 / 118 cm | N/A / 18 | 0.88 | **172°** / 193 | Amalgamated eastern side of the Wildcat |
| ETF | Eastern Thrust Fault | North | 252 | 184 | 150 / 61 cm | 44 9 | 0.80 | **164°** / 127 | Transitional central zone of the Wildcat |
| WTF | Western Thrust Fault | North | 224 | 181 | 120 / 78 cm | 2.6 36 | 0.62 | **128°** / 106 | Western bedded side of the Wildcat |
| CC | Central Canyon | Central | 330 | 294 | 2 m / 97 cm | 2.4 14 | 0.70 | **157°** / 189 | Full thickness of the Wildcat; bedded W side |
| SSM | South Side Margin | South | 63 | 23 | N/A / 74 cm | 1.7 32 | 0.59 | **164°** / 42 | Channel fill & abandonment IIIsm facies at E margin |
| H2O | Waterfall | South | 95 | 95 | 1.6 / 1.1 m | N/A / 17 cm | 0.90 | **157°** / 31 | Amalgamated eastern side |
| Rocas | Rocas dip face | South | 315 | 315 | 1.9 / 1.2 m | 3.2 / 0.5 m | 0.95 | **177°** / 88 | Full preserved thickness of the Wildcat channel |
| SC | Snowy Cliff | South | 65 | 0 | 3.8 / 1.3 m | 50 / 20 cm | 0.83 | **197°** / 29 | Undifferentiated channel fill above the Wildcat |
| DC1 | Downcutting 1 | South | 92 | 0 | 100 / 57 cm | 118 / 7 cm | 0.68 | **165°** / 91 | Undifferentiated channel fill above the Wildcat |
| DC2 | Downcutting 2 | South | 18 | 0 | 96 / 49 cm | 200 / 7 cm | 0.76 | **117°** / 4 | Undifferentiated channel fill above the Wildcat |
| SW | Slurry Wall | North | 69 | 0 | 1.6 / 1 m | 320 / 11 cm | 0.81 | -- | Undifferentiated channel fill above the Wildcat |

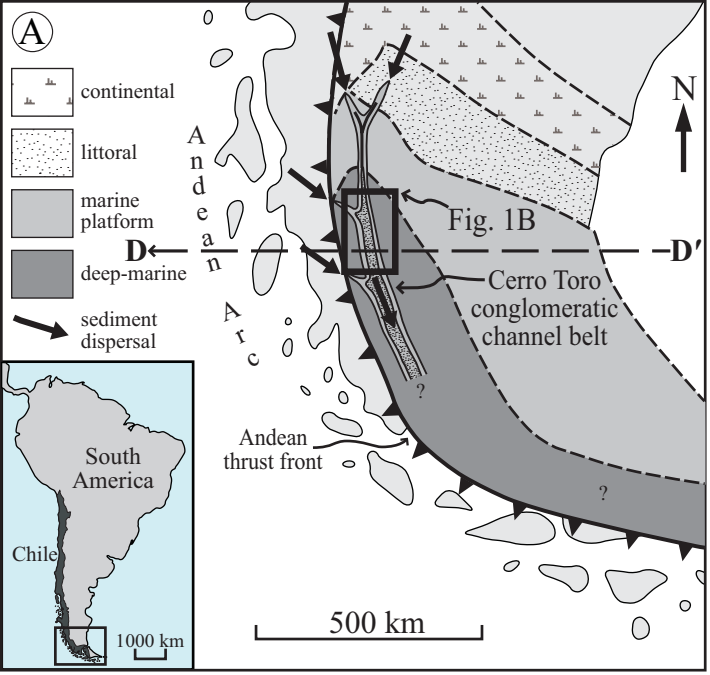
A
continental
littoral
marine platform
deep-marine
sediment dispersal
Andean Arc
N
D
D′
Fig. 1B
Cerro Toro conglomeratic channel belt
Andean thrust front
South America
Chile
1000 km
500 km

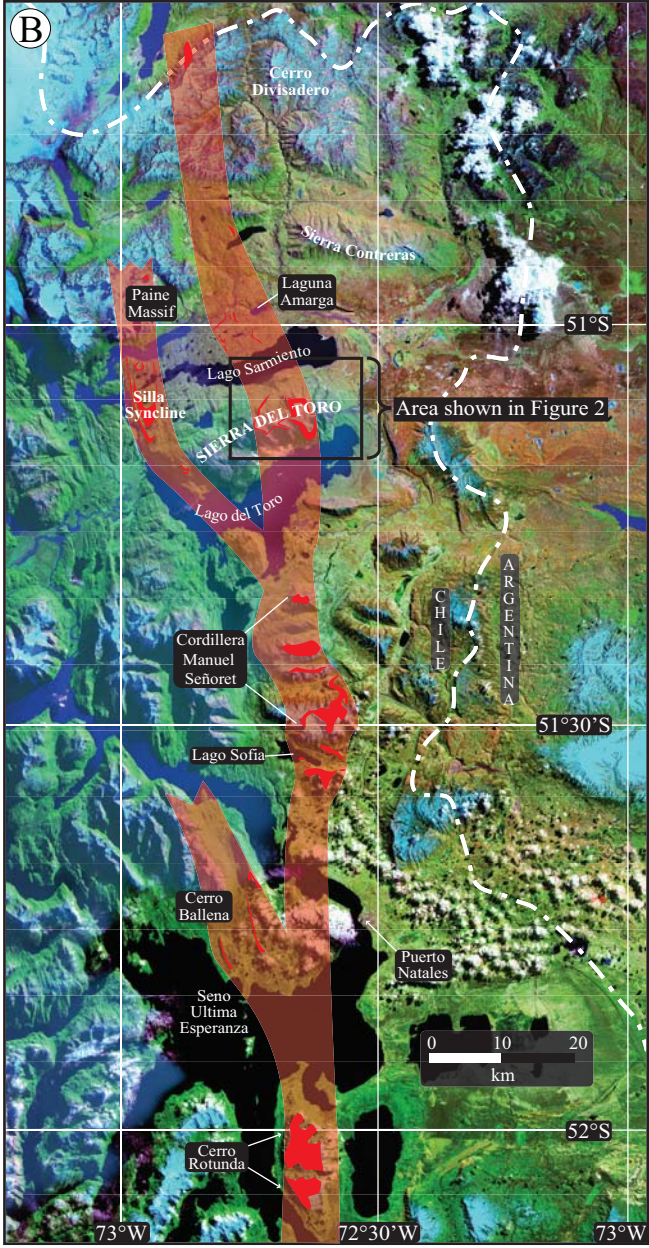
B
Cerro Divisadero
Sierra Contreras
Paine Massif
Laguna Amarga
51°S
Lago Sarmiento
Silla Syncline
SIERRA DEL TORO
Area shown in Figure 2
Lago del Toro
CHILE
ARGENTINA
Cordillera Manuel Señoret
51°30'S
Lago Sofía
Cerro Ballena
Puerto Natales
Seno Ultima Esperanza
0 10 20
km
52°S
Cerro Rotunda
73°W
72°30'W
73°W

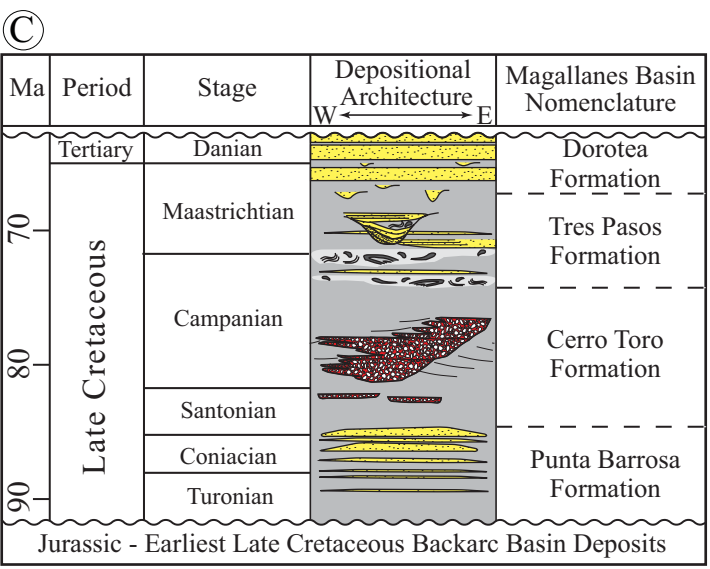
C
Ma
Period
Stage
Depositional Architecture
W
E
Magallanes Basin Nomenclature
Tertiary
Danian
Dorotea Formation
Late Cretaceous
Maastrichtian
Tres Pasos Formation
70
Campanian
Cerro Toro Formation
80
Santonian
Coniacian
Punta Barrosa Formation
Turonian
90
Jurassic - Earliest Late Cretaceous Backarc Basin Deposits

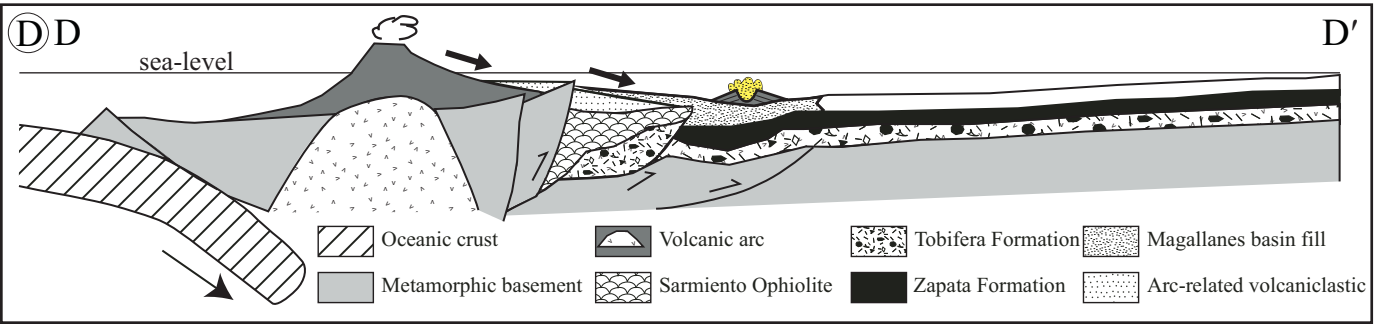
D
D
D′
sea-level
Oceanic crust
Metamorphic basement
Volcanic arc
Sarmiento Ophiolite
Tobifera Formation
Zapata Formation
Magallanes basin fill
Arc-related volcaniclastic

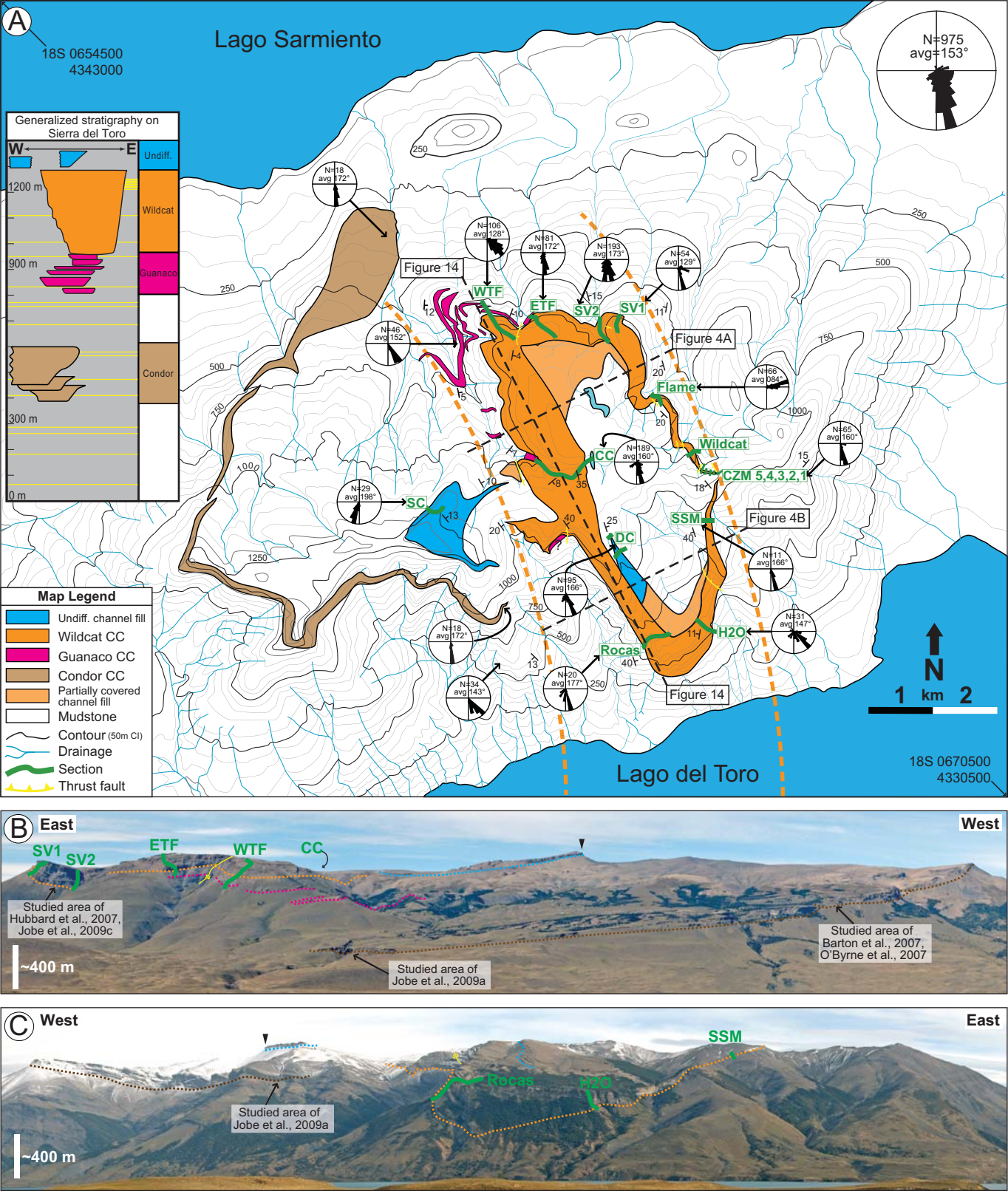
A
18S 0654500
4343000
Lago Sarmiento
N=975
avg=153°
Generalized stratigraphy on
Sierra del Toro
W
E
1200 m
900 m
300 m
0 m
Undiff.
Wildcat
Guanaco
Condor
Figure 14
WTF
ETF
SV2
SV1
Figure 4A
Flame
Wildcat
CC
CZM 5,4,3,2,1
SC
SSM
Figure 4B
DC
H2O
Rocas
Figure 14
Lago del Toro
18S 0670500
4330500
N
1 km 2
Map Legend
Undiff. channel fill
Wildcat CC
Guanaco CC
Condor CC
Partially covered channel fill
Mudstone
Contour (50m CI)
Drainage
Section
Thrust fault
B
East
West
SV1
SV2
ETF
WTF
CC
Studied area of Hubbard et al., 2007, Jobe et al., 2009c
~400 m
Studied area of Jobe et al., 2009a
Studied area of Barton et al., 2007, O'Byrne et al., 2007
C
West
East
SSM
Rocas
H2O
Studied area of Jobe et al., 2009a
~400 m

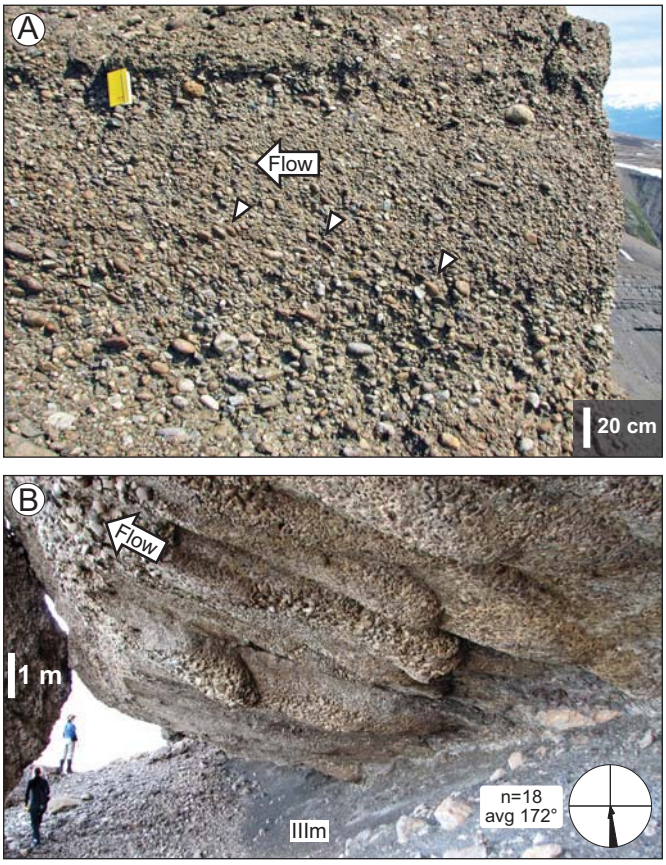
A
Flow
20 cm
B
Flow
1 m
IIIm
n=18
avg 172°

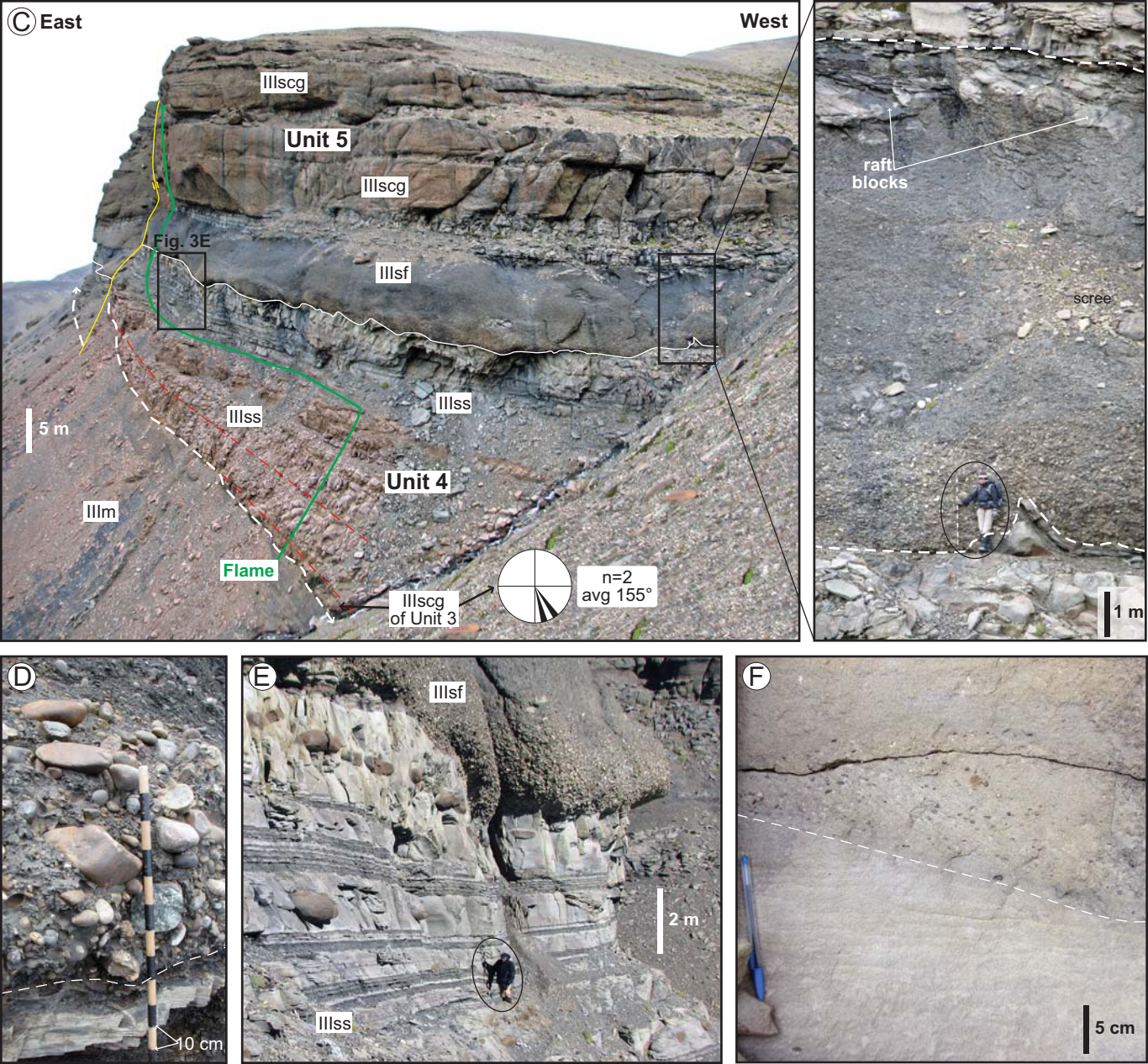
C
East
West
IIIscg
Unit 5
IIIscg
Fig. 3E
IIIsf
IIIss
IIIss
5 m
IIIm
Unit 4
Flame
IIIscg
of Unit 3
n=2
avg 155°
raft
blocks
scree
1 m
D
10 cm
E
IIIsf
2 m
IIIss
F
5 cm

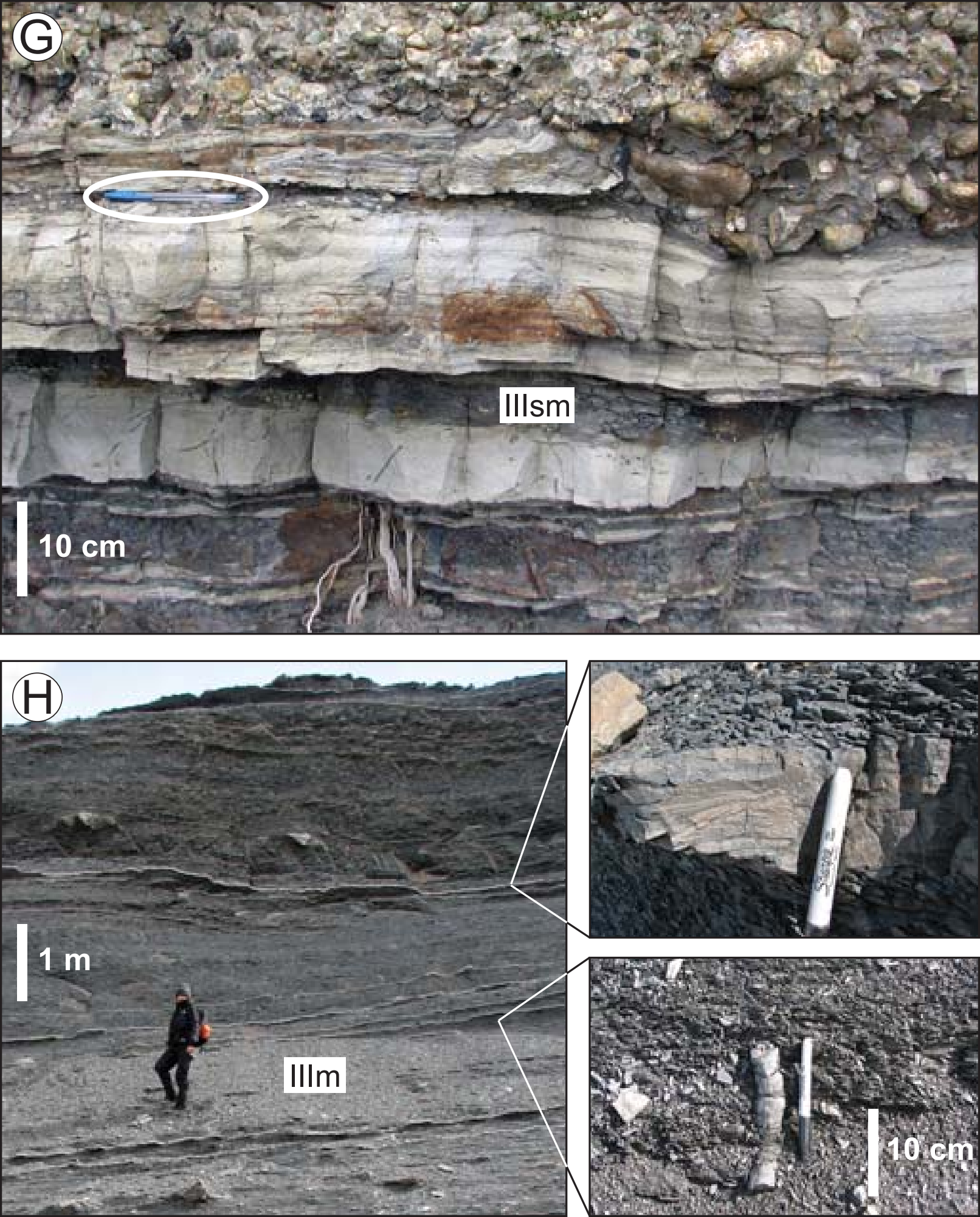
G
IIIsm
10 cm
H
1 m
IIIm
10 cm

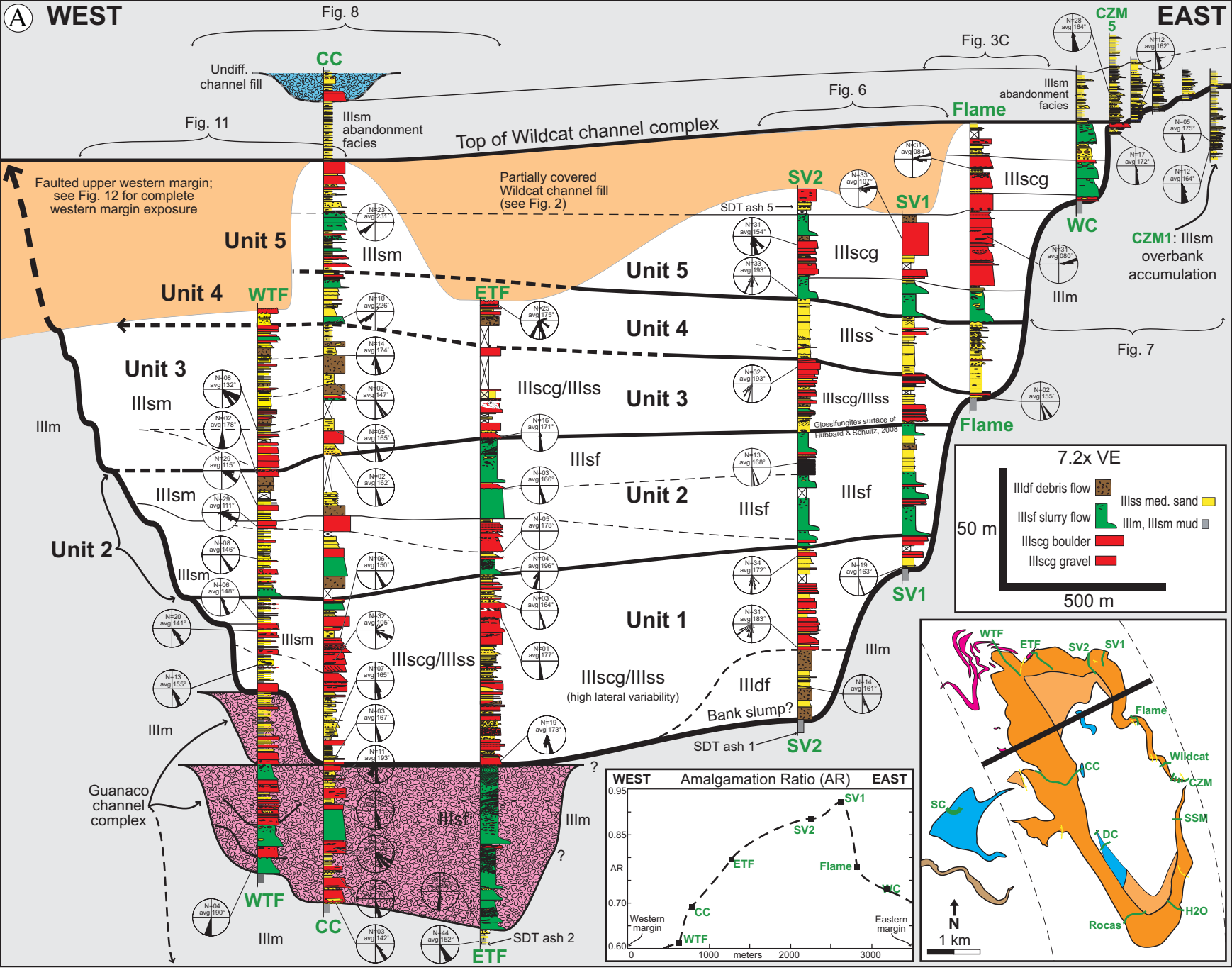
A
WEST
EAST
Fig. 8
Fig. 3C
Fig. 6
Fig. 11
Fig. 7
CC
CZM 5
Undiff. channel fill
IIIsm abandonment facies
Top of Wildcat channel complex
Flame
WC
CZM1: IIIsm overbank accumulation
Faulted upper western margin; see Fig. 12 for complete western margin exposure
Partially covered Wildcat channel fill (see Fig. 2)
SV2
SV1
SDT ash 5
Unit 5
Unit 4
Unit 3
Unit 2
Unit 1
WTF
ETF
IIIsm
IIIm
IIIscg
IIIss
IIIscg/IIIss
IIIsf
IIIdf
Glossifungites surface of Hubbard & Schultz, 2008
Guanaco channel complex
Bank slump?
SDT ash 1
SDT ash 2
(high lateral variability)
7.2x VE
50 m
500 m
IIIdf debris flow
IIIsf slurry flow
IIIscg boulder
IIIscg gravel
IIIss med. sand
IIIm, IIIsm mud
Amalgamation Ratio (AR)
AR
Western margin
Eastern margin
meters
SC
DC
SSM
H2O
Rocas
Wildcat
N
1 km

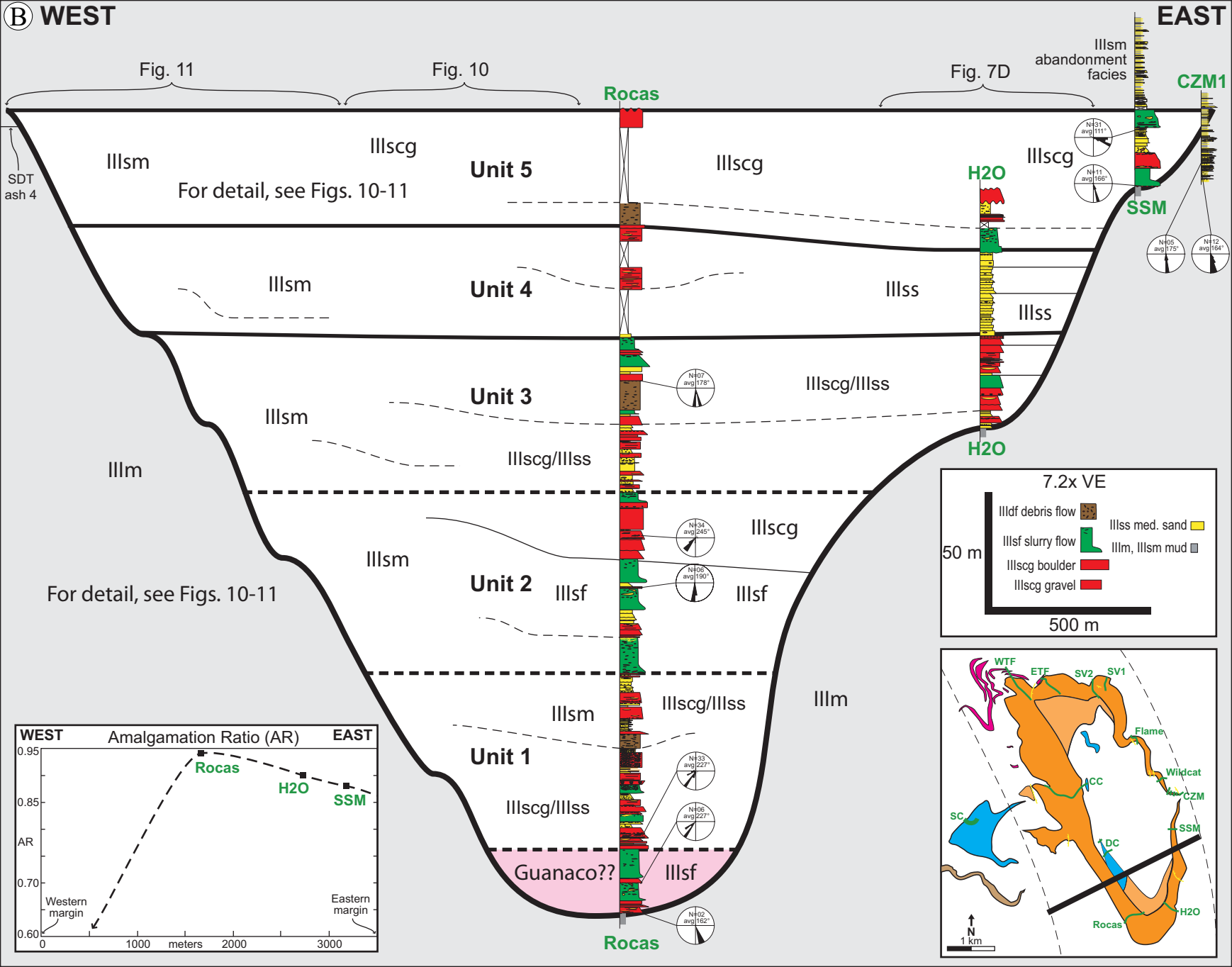
B WEST
EAST
Fig. 11
Fig. 10
Fig. 7D
Rocas
IIIsm abandonment facies
CZM1
SDT ash 4
IIIsm
IIIscg
Unit 5
For detail, see Figs. 10-11
IIIscg
H2O
IIIscg
SSM
IIIsm
Unit 4
IIIss
IIIss
Unit 3
IIIscg/IIIss
IIIsm
IIIscg/IIIss
IIIm
H2O
7.2x VE
IIIdf debris flow
IIIss med. sand
IIIsf slurry flow
IIIm, IIIsm mud
IIIscg boulder
IIIscg gravel
50 m
500 m
IIIscg
IIIsm
Unit 2
IIIsf
IIIsf
For detail, see Figs. 10-11
IIIsm
IIIscg/IIIss
IIIm
Unit 1
IIIscg/IIIss
Guanaco??
IIIsf
Rocas
Amalgamation Ratio (AR)
WEST
EAST
0.95
0.85
0.70
0.60
AR
Rocas
H2O
SSM
Western margin
Eastern margin
0
1000
meters
2000
3000
WTF
ETF
SV2
SV1
Flame
Wildcat
CC
CZM
SC
SSM
DC
H2O
Rocas
N
1 km

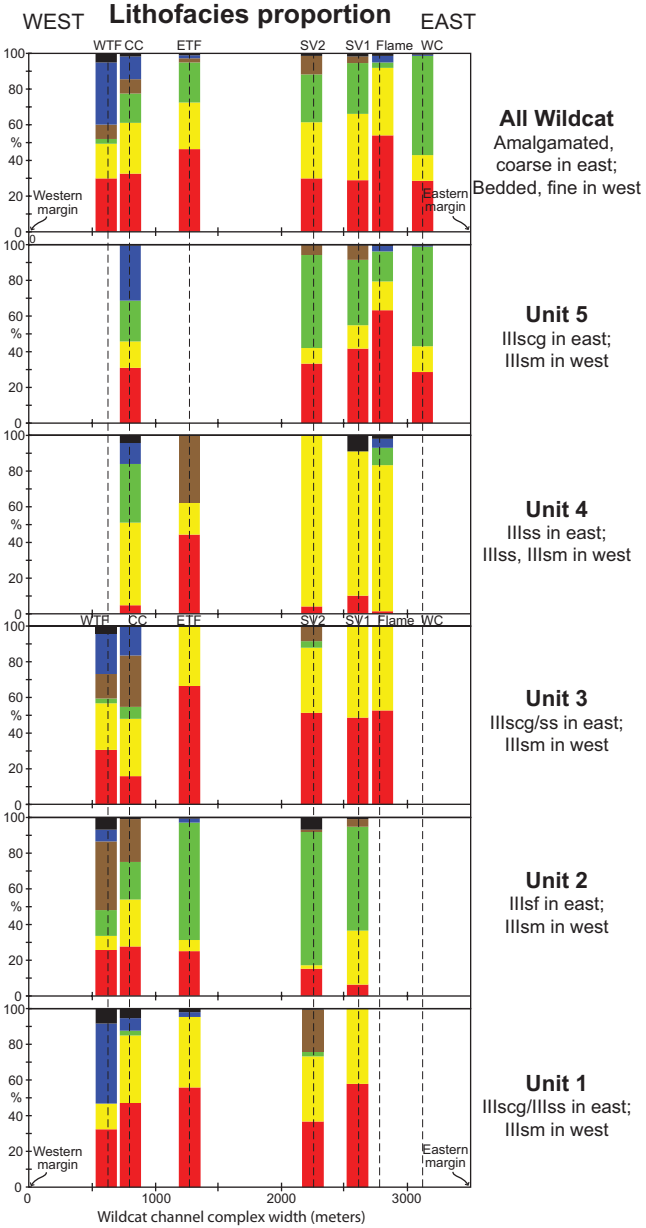
WEST
Lithofacies proportion
EAST
WTF
CC
ETF
SV2
SV1
Flame
WC
%
Western margin
Eastern margin
All Wildcat
Amalgamated, coarse in east; Bedded, fine in west
Unit 5
IIIscg in east; IIIsm in west
Unit 4
IIIss in east; IIIss, IIIsm in west
Unit 3
IIIscg/ss in east; IIIsm in west
Unit 2
IIIsf in east; IIIsm in west
Unit 1
IIIscg/IIIss in east; IIIsm in west
0
1000
2000
3000
Wildcat channel complex width (meters)
IIIm mudstone with rare sandstone
IIIsm sandstone & mudstone
IIIdf debris-flow conglomerate
IIIsf slurry-flow conglomerate
IIIss thick-bedded amalgamated sandstone
IIIscg clast-supported conglomerate

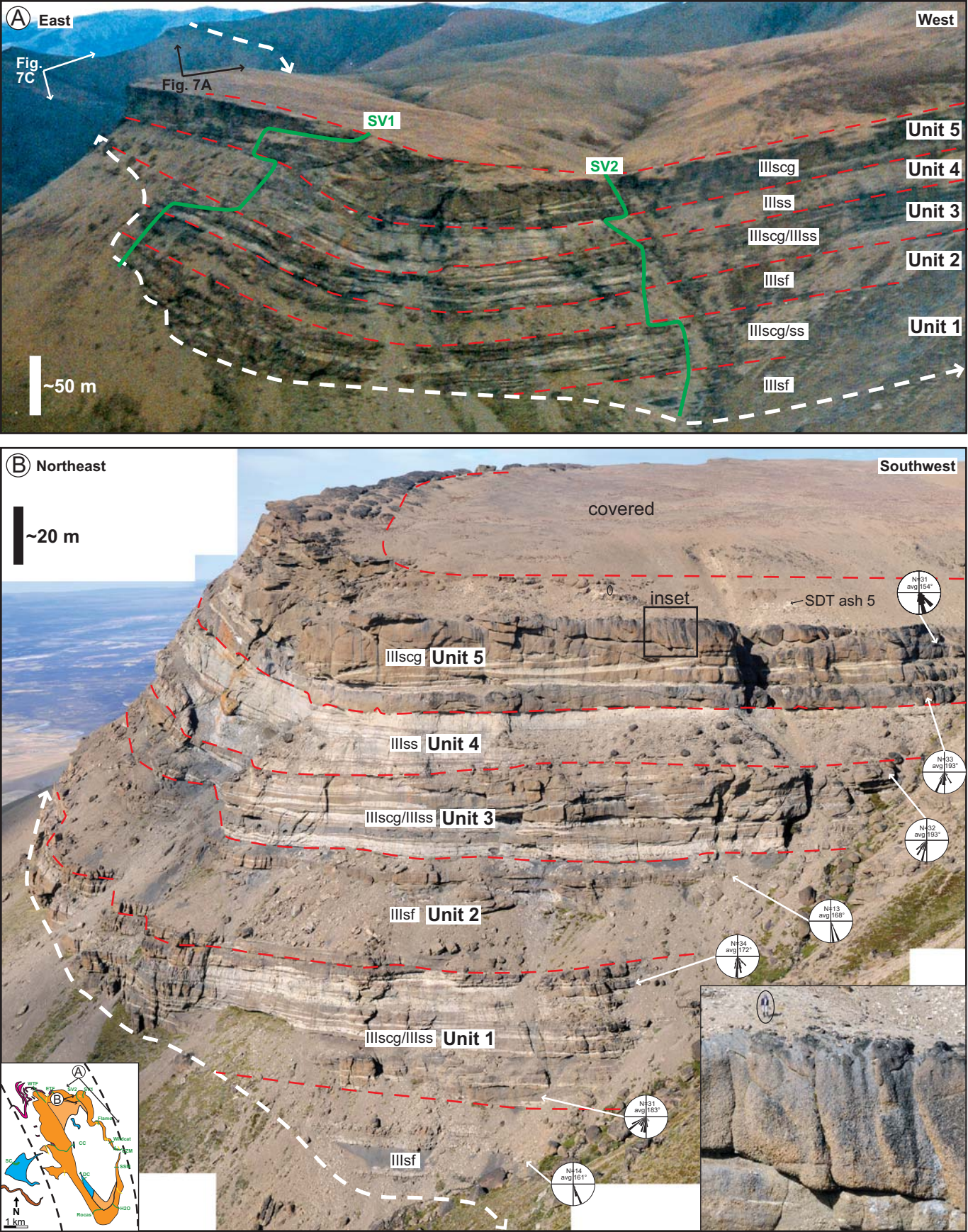
A
East
West
Fig. 7C
Fig. 7A
SV1
SV2
Unit 5
Unit 4
Unit 3
Unit 2
Unit 1
IIIscg
IIIss
IIIscg/IIIss
IIIsf
IIIscg/ss
IIIsf
~50 m
B
Northeast
Southwest
~20 m
covered
inset
SDT ash 5
IIIscg Unit 5
IIIss Unit 4
IIIscg/IIIss Unit 3
IIIsf Unit 2
IIIscg/IIIss Unit 1
IIIsf
N=31 avg 154°
N=33 avg 193°
N=32 avg 193°
N=13 avg 168°
N=34 avg 172°
N=31 avg 183°
N=14 avg 161°
WTF
ETF
SV2
SV1
Flame
Wildcat
CC
SC
SSM
LDC
H2O
Rocas
N
1 km

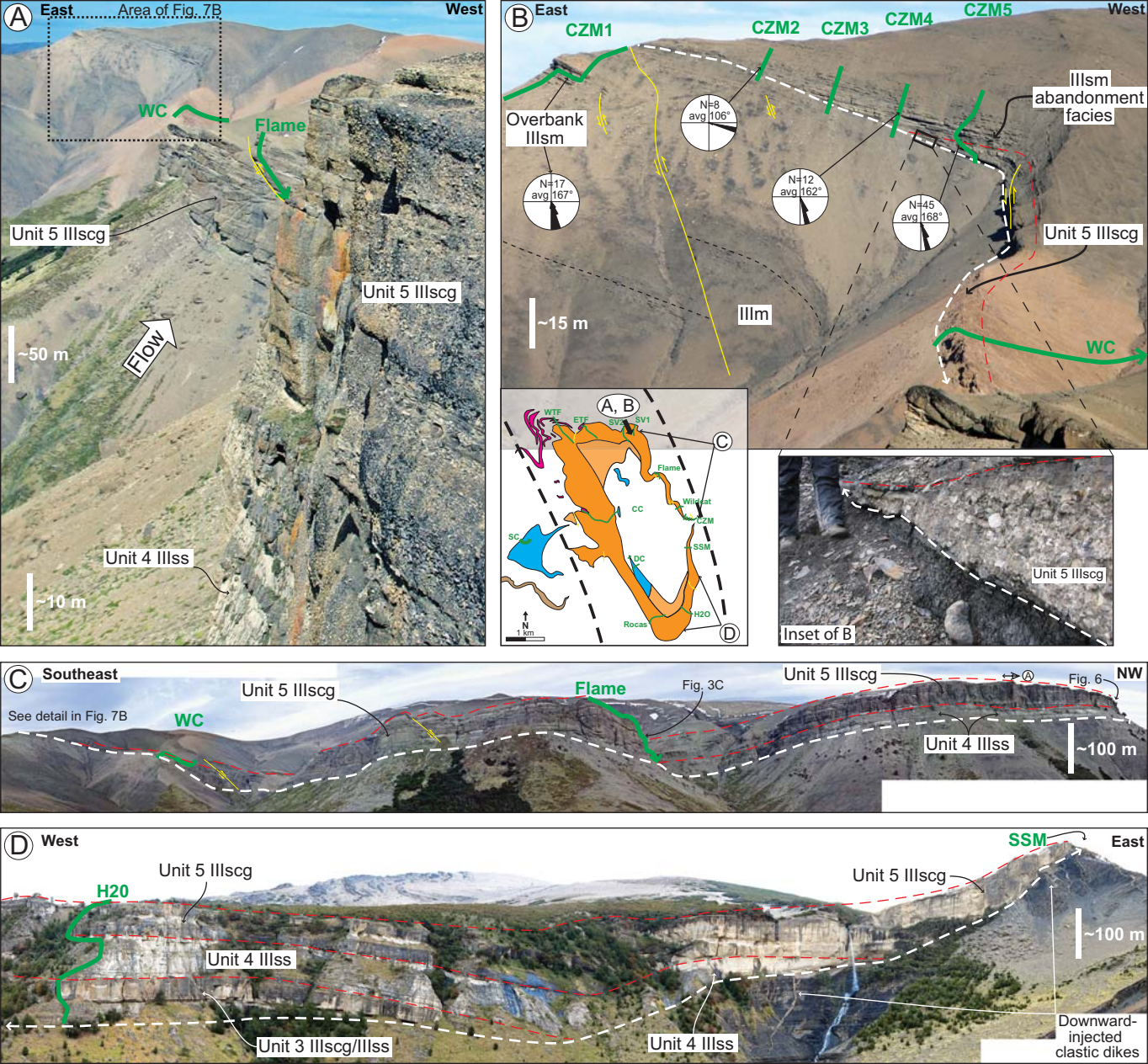
A
East
Area of Fig. 7B
West
WC
Flame
Unit 5 IIIscg
Unit 5 IIIscg
~50 m
Flow
Unit 4 IIIss
~10 m
B
East
CZM1
CZM2
CZM3
CZM4
CZM5
West
Overbank IIIsm
IIIsm abandonment facies
N=8 avg 106°
N=17 avg 167°
N=12 avg 162°
N=45 avg 168°
Unit 5 IIIscg
~15 m
IIIm
WC
A, B
C
D
WTF
ETF
SV2
SV1
Flame
Wildcat
CC
CZM
SSM
SC
DC
H2O
Rocas
N
1 km
Unit 5 IIIscg
Inset of B
C
Southeast
Unit 5 IIIscg
Flame
Fig. 3C
Unit 5 IIIscg
Fig. 6
NW
See detail in Fig. 7B
WC
Unit 4 IIIss
~100 m
D
West
SSM
East
Unit 5 IIIscg
H20
Unit 5 IIIscg
Unit 4 IIIss
~100 m
Unit 3 IIIscg/IIIss
Unit 4 IIIss
Downward-injected clastic dikes

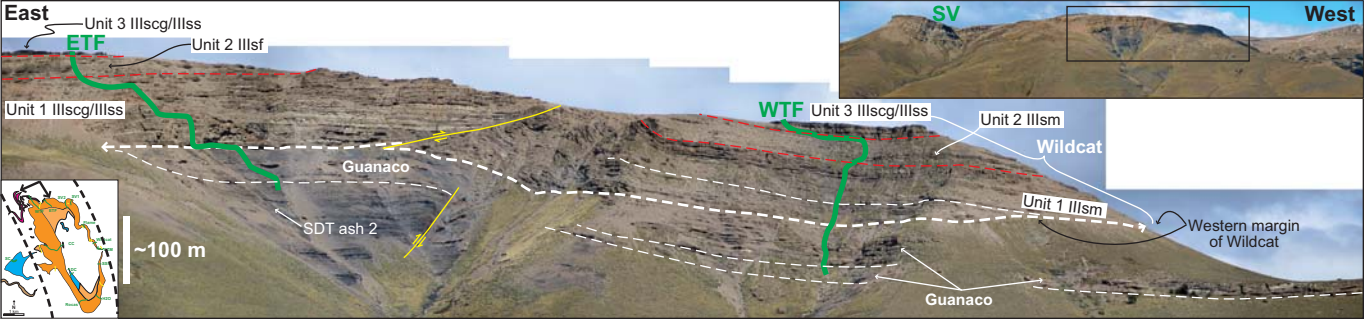
East
Unit 3 IIIscg/IIIss
ETF
Unit 2 IIIsf
Unit 1 IIIscg/IIIss
Guanaco
SDT ash 2
~100 m
SV
West
WTF
Unit 3 IIIscg/IIIss
Unit 2 IIIsm
Wildcat
Unit 1 IIIsm
Western margin
of Wildcat
Guanaco

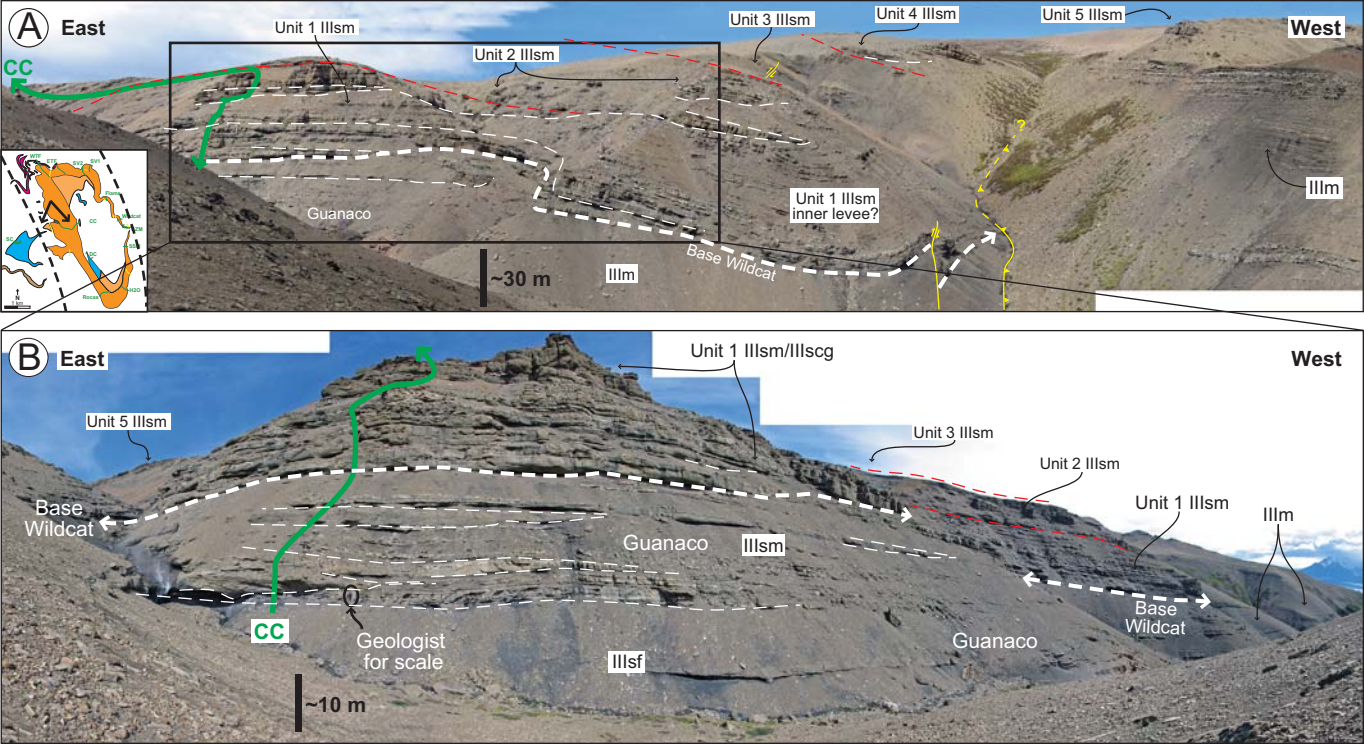
A
East
West
Unit 1 IIIsm
Unit 2 IIIsm
Unit 3 IIIsm
Unit 4 IIIsm
Unit 5 IIIsm
CC
Guanaco
Unit 1 IIIsm
inner levee?
IIIm
Base Wildcat
~30 m
IIIm
B
East
West
Unit 1 IIIsm/IIIscg
Unit 5 IIIsm
Unit 3 IIIsm
Unit 2 IIIsm
Unit 1 IIIsm
IIIm
Base
Wildcat
Guanaco
IIIsm
CC
Geologist
for scale
IIIsf
Guanaco
Base
Wildcat
~10 m

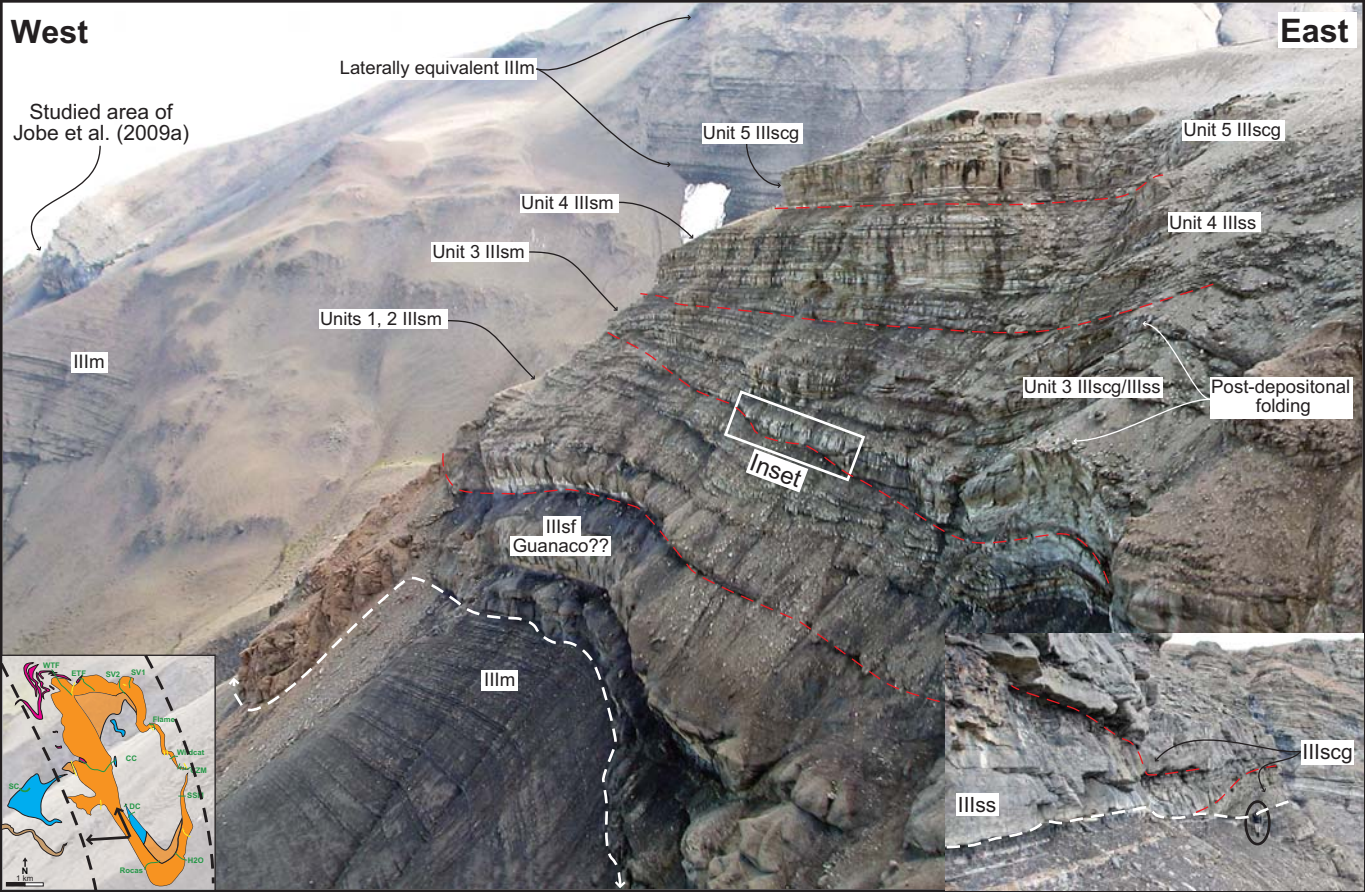
West
East
Laterally equivalent IIIm
Studied area of Jobe et al. (2009a)
Unit 5 IIIscg
Unit 5 IIIscg
Unit 4 IIIsm
Unit 4 IIIss
Unit 3 IIIsm
Units 1, 2 IIIsm
IIIm
Unit 3 IIIscg/IIIss
Post-depositonal folding
Inset
IIIsf
Guanaco??
IIIm
IIIscg
IIIss
WTF
ETF
SV2
SV1
Flamo
Wildcat
CC
ZM
SS
SC
TDC
H2O
Rocas
N
1 km

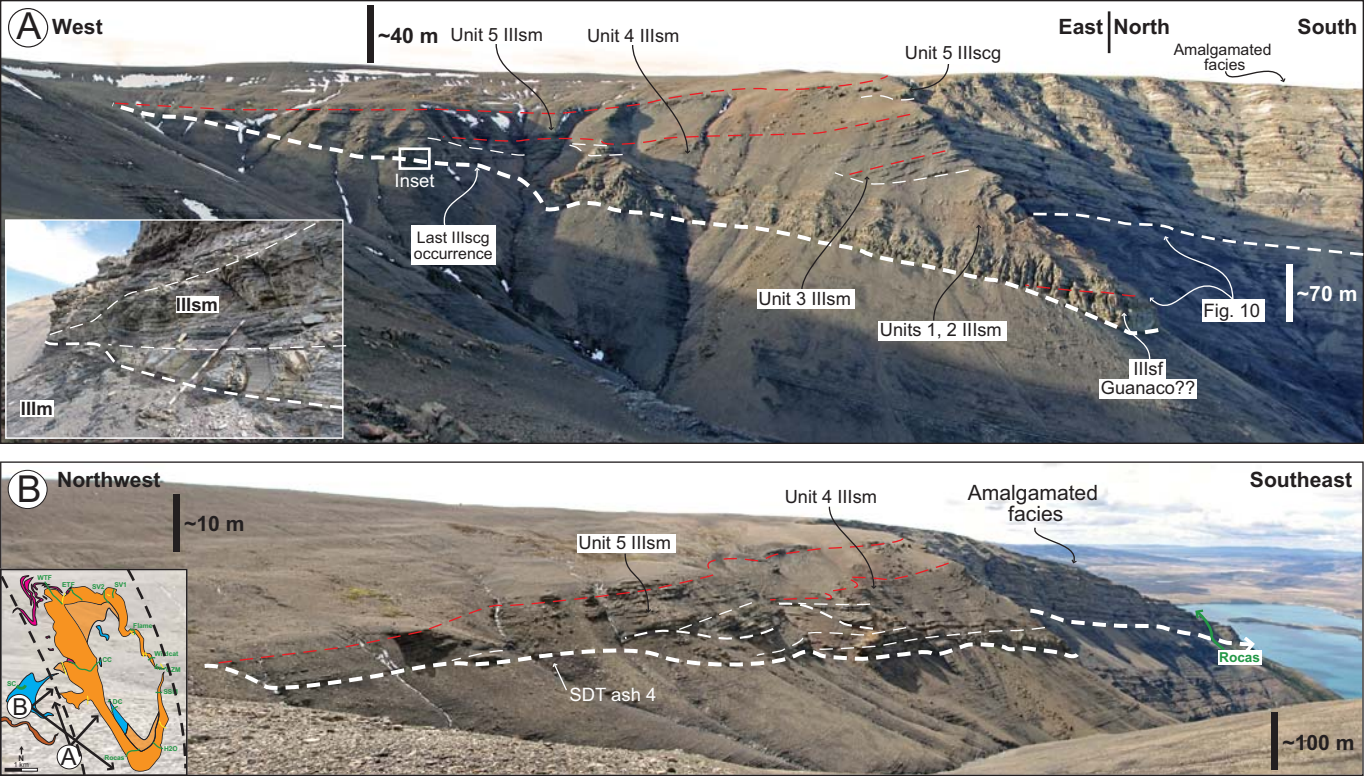
A
West
~40 m
Unit 5 IIIsm
Unit 4 IIIsm
East
North
South
Unit 5 IIIscg
Amalgamated facies
Inset
Last IIIscg occurrence
IIIsm
IIIm
Unit 3 IIIsm
Units 1, 2 IIIsm
Fig. 10
~70 m
IIIsf Guanaco??
B
Northwest
~10 m
Unit 4 IIIsm
Amalgamated facies
Unit 5 IIIsm
Southeast
Rocas
SDT ash 4
~100 m
WTF
ETF
SV2
SV1
Fiume
Wildcat
SC
B
A
Rocas
N

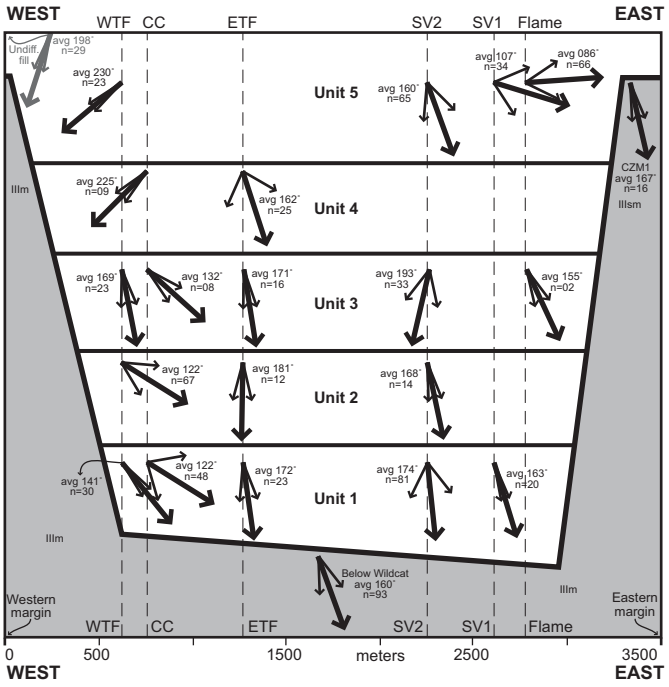
WEST
EAST
WTF
CC
ETF
SV2
SV1
Flame
Undiff. fill
avg 198˚ n=29
avg 230˚ n=23
Unit 5
avg 160˚ n=65
avg 107˚ n=34
avg 086˚ n=66
CZM1 avg 167˚ n=16
IIIsm
IIIm
avg 225˚ n=09
avg 162˚ n=25
Unit 4
avg 169˚ n=23
avg 132˚ n=08
avg 171˚ n=16
Unit 3
avg 193˚ n=33
avg 155˚ n=02
avg 122˚ n=67
avg 181˚ n=12
Unit 2
avg 168˚ n=14
avg 141˚ n=30
avg 122˚ n=48
avg 172˚ n=23
Unit 1
avg 174˚ n=81
avg 163˚ n=20
Below Wildcat avg 160˚ n=93
Western margin
Eastern margin
0
500
1500
meters
2500
3500

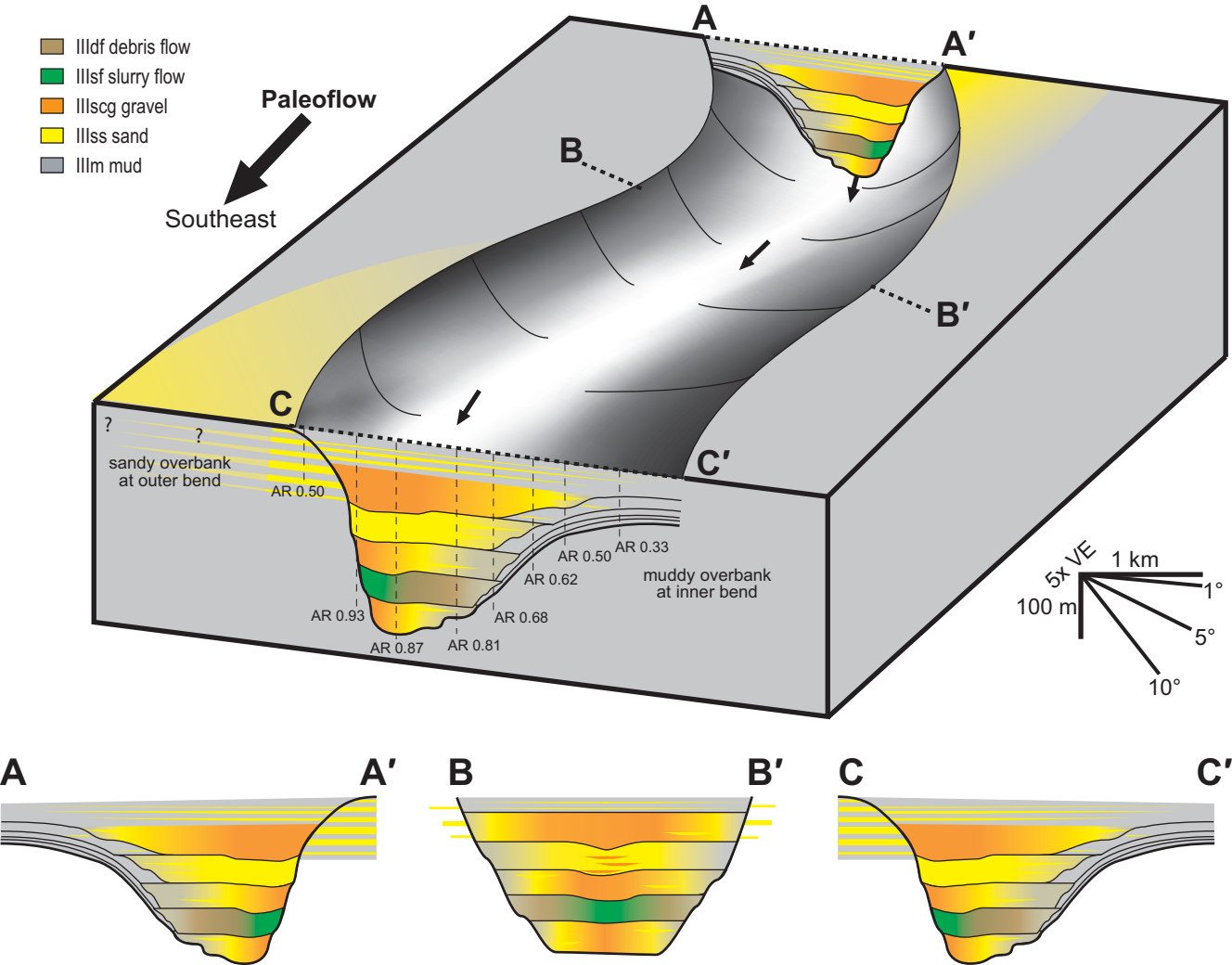
IIIdf debris flow
IIIsf slurry flow
IIIscg gravel
IIIss sand
IIIm mud
Paleoflow
Southeast
A
A′
B
B′
C
C′
?
?
sandy overbank
at outer bend
AR 0.50
AR 0.93
AR 0.87
AR 0.81
AR 0.68
AR 0.62
AR 0.50
AR 0.33
muddy overbank
at inner bend
5x VE
1 km
100 m
1°
5°
10°
A
A′
B
B′
C
C′

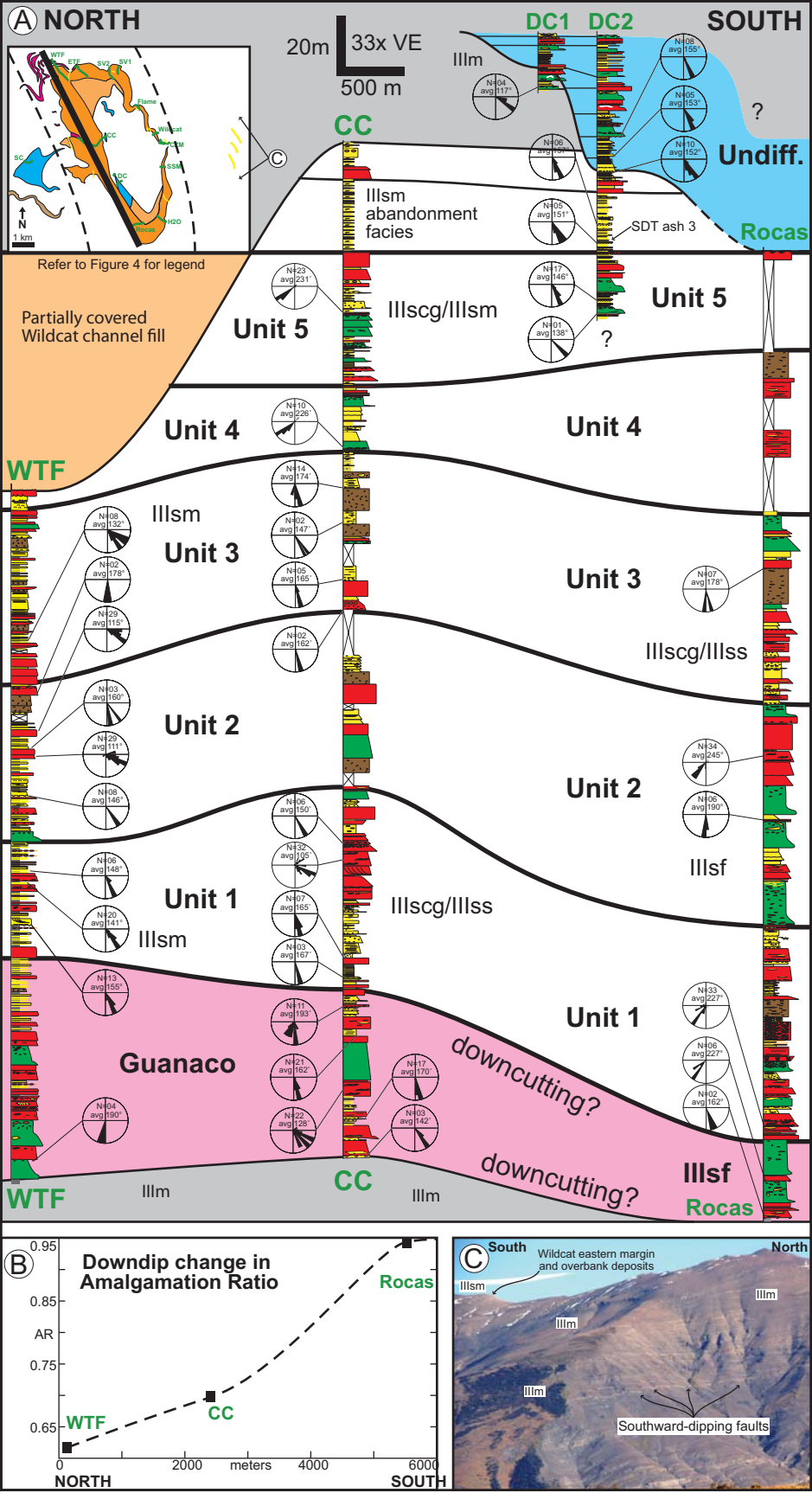
A NORTH
SOUTH
20m
33x VE
500 m
DC1
DC2
IIIm
CC
IIIsm
abandonment
facies
SDT ash 3
Undiff.
Rocas
Refer to Figure 4 for legend
Partially covered
Wildcat channel fill
Unit 5
IIIscg/IIIsm
Unit 4
WTF
IIIsm
Unit 3
Unit 2
Unit 1
IIIsm
Guanaco
IIIscg/IIIss
IIIsf
downcutting?
WTF
IIIm
CC
IIIm
B
Downdip change in
Amalgamation Ratio
0.95
0.85
AR
0.75
0.65
WTF
CC
Rocas
0
2000
meters
4000
6000
NORTH
SOUTH
C
South
North
Wildcat eastern margin
and overbank deposits
IIIsm
IIIm
Southward-dipping faults